HAL open science

Anisotropic optical trapping as a manifestation of the complex electronic structure of ultracold lanthanide atoms: The example of holmium

Hui Li, Jean-François Wyart, Olivier Dulieu, Maxence Lepers

To cite this version:

Hui Li, Jean-François Wyart, Olivier Dulieu, Maxence Lepers. Anisotropic optical trapping as a manifestation of the complex electronic structure of ultracold lanthanide atoms: The example of holmium. Physical Review A, 2017, 95 (6), 10.1103/PhysRevA.95.062508 . hal-02265753

HAL Id: hal-02265753

https://hal.science/hal-02265753v1

Submitted on 27 May 2021

HAL is a multi-disciplinary open access archive for the deposit and dissemination of scientific research documents, whether they are published or not. The documents may come from teaching and research institutions in France or abroad, or from public or private research centers.

L'archive ouverte pluridisciplinaire **HAL**, est destinée au dépôt et à la diffusion de documents scientifiques de niveau recherche, publiés ou non, émanant des établissements d'enseignement et de recherche français ou étrangers, des laboratoires publics ou privés.

Anisotropic optical trapping as a manifestation of the complex electronic structure of ultracold lanthanide atoms: The example of holmium

Hui Li,[1] Jean-François Wyart,[1,2] Olivier Dulieu,[1] and Maxence Lepers[1,*]
[1]*Laboratoire Aimé Cotton, CNRS, Université Paris-Sud, ENS Paris-Saclay, Université Paris-Saclay, 91405 Orsay, France*
[2]*LERMA, Observatoire de Paris–Meudon, PSL Research University, Sorbonne Universités, UPMC Université Paris 6, CNRS UMR8112, 92195 Meudon, France*
(Received 13 April 2017; published 26 June 2017)

The efficiency of optical trapping is determined by the atomic dynamic dipole polarizability, whose real and imaginary parts are associated with the potential energy and photon-scattering rate, respectively. In this article we develop a formalism to calculate analytically the real and imaginary parts of the scalar, vector, and tensor polarizabilities of lanthanide atoms. We assume that the sum-over-state formula comprises only transitions involving electrons in the valence orbitals like $6s$, $5d$, $6p$, and $7s$, while transitions involving $4f$ core electrons are neglected. Applying this formalism to the ground level of configuration $4f^q6s^2$, we restrict the sum to transitions implying the $4f^q6s6p$ configuration, which yields polarizabilities depending on two parameters: an effective transition energy and an effective transition dipole moment. Then, by introducing configuration-interaction mixing between $4f^q6s6p$ and other configurations, we demonstrate that the imaginary part of the scalar, vector, and tensor polarizabilities is very sensitive to configuration-interaction coefficients, whereas the real part is not. The magnitude and anisotropy of the photon-scattering rate are thus strongly related to the details of the atomic electronic structure. Those analytical results agree with our detailed electronic-structure calculations of the energy levels, Landé g factors, transition probabilities, polarizabilities, and van der Waals C_6 coefficients, previously performed on erbium and dysprosium and presently performed on holmium. Our results show that, although the density of states decreases with increasing q, the configuration interaction between $4f^q6s6p$, $4f^{q-1}5d6s^2$, and $4f^{q-1}5d^26s$ is surprisingly stronger in erbium ($q = 12$) than in holmium ($q = 11$), itself stronger than in dysprosium ($q = 10$).

DOI: 10.1103/PhysRevA.95.062508

I. INTRODUCTION

The physics of ultracold gases has evolved rapidly and is poised to enter a new, promising regime, where complex atomic and molecular species can be cooled and studied extensively. Lanthanide atoms, with a strong magnetic moment and a large orbital angular momentum, are extreme examples of such complex species. In fact, the interest in ultracold lanthanide atoms is motivated by several topics in current research, including ultracold collisions and quantum chaos [1–3], dipolar quantum gases with large magnetic moments and strong dipole-dipole interactions [4–8], many-body quantum systems [9,10], exotic quantum phases [11–13] like stable quantum droplets [14–16], synthetic gauge fields [17,18], and optical clocks [19–21]. Recent progress in laser cooling and magneto-optical trapping of high-atomic-number (high-Z) lanthanides [22,23], including dysprosium (Dy) [24–27], erbium (Er) [28–30], holmium (Ho) [31], and thulium (Tm) [32] is paving the way towards these investigations. In addition, both Bose-Einstein condensates and quantum-degenerate Fermi gases have been produced in isotopes of Dy [4,33,34] and Er [35,36].

The ground level of holmium is characterized by the electronic configuration [Xe]$4f^{11}6s^2$ and electronic angular momentum $J = 15/2$. Due to the nuclear spin $I = 7/2$ of its only stable (bosonic) isotope ^{165}Ho, holmium is the atom possessing the largest number of hyperfine sublevels in the electronic ground level, namely, $(2J + 1) \times (2I + 1) = 128$. This rich structure is likely to be exploited in quantum information [37,38]. Like other lanthanides, the complex electronic structure of holmium induces a large magnetic dipole moment ($9\,\mu_B$),which makes it an interesting candidate for the investigation of anisotropic interactions between atoms [39,40]. Recently the holmium single magnetic atom and holmium molecular nanomagnet were also presented as competing candidates for the realization of quantum bits [41,42].

Many of the applications listed above involve optically trapped ultracold atoms. The trapping efficiency is determined by the interaction between the atoms and the electromagnetic field [43,44]. The microscopic property characterizing the atomic response is the (complex) dynamic dipole polarizability (DDP). On the one hand, the field induces a potential energy, i.e., an ac-Stark shift, in the atoms, which is proportional to the real part of the DDP. On the other hand, the field also induces photon scattering, whose rate is proportional to the imaginary part of the DDP. In ultracold experiments, it is necessary to characterize the photon-scattering rate, as it provokes heating of the sample and trap losses [44]. Beyond trapping itself, the real part of the vector and tensor DDPs is also necessary to determine the Raman coupling strengths between different Zeeman sublevels, which was proposed for the implementation of synthetic gauge fields [17,18]. In our previous works on Er [45] and Dy [46], we have shown that, far from resonant frequencies, the ac-Stark shift only weakly depends on the field polarization and atomic Zeeman sublevel, despite the absence of spherical symmetry in the $4f$-electron wave functions. We have revealed the inverse situation for photon scattering, as the imaginary part of the vector and tensor DDPs represents significant fractions of the scalar one.

*maxence.lepers@u-psud.fr

 ©2017 American Physical Society

This opens the possibility of controlling the trap heating and losses with an appropriate field polarization. However, the vector-to-scalar and tensor-to-scalar ratios vary strongly from Dy to Er, which is still unexplained.

Understanding the origin of that difference is a major motivation of the present work. Moreover, ultracold experiments may require characterization of the optical trapping of atomic excited levels with energies up to 25 000 cm^{-1} above ground level. Calculating the DDP of such levels with the sum-over-state formula requires modeling highly excited levels, roughly up to 60 000 cm^{-1} above ground level, which is a hard task for the most complex spectra of lanthanide atoms. Therefore, in this article, we present a simplified model of the DDP based on the sum-over-state formula, where we suppose that the only contributions come from transitions involving valence electrons like $6s$, $6p$, $5d$, and $7s$ and where we ignore transitions involving $4f$ core electrons. Assuming that all the levels of a given configuration have similar energies, we obtain analytical expressions of the DDPs of an arbitrary level, depending on a restricted number of effective parameters. Focusing on the ground level of the configuration $[\mathrm{Xe}]4f^q6s^2$ ($q = 10$, 11, and 12 for Dy, Ho, and Er, respectively), we take into account only the excitation from the $6s$ to the $6p$ orbital, and not the excitation from the $4f$ to the $5d$ orbital. We demonstrate that the real part of the DDP is not influenced by the configuration interaction (CI) between $[\mathrm{Xe}]4f^q6s6p$ and other configurations like $[\mathrm{Xe}]4f^{q-1}5d6s^2$ and $[\mathrm{Xe}]4f^{q-1}5d^26s$. Our model also shows that the real part of the vector and tensor ground-level DDPs vanish. By contrast, the imaginary part of the DDPs is very sensitive to CI, in particular, to the weight of the $[\mathrm{Xe}]4f^q6s6p$ configuration in excited levels. We demonstrate that strong CI mixing tends to increase the vector and tensor DDPs with respect to the scalar one. Surprisingly, CI mixing turns out to be larger for Er than for Ho, and for Ho than for Dy, although the energy spectrum of Dy is the densest one.

In order to check the validity of those conclusions, we perform a full numerical modeling of holmium spectrum, including energy levels, transition probabilities, polarizabilities, and van der Waals C_6 coefficients, complementing our previous studies on erbium [45] and dysprosium [46]. The DDPs and C_6 coefficients are calculated using the sum formula involving transition energies and transition dipole moments extracted from our computed transition probabilities. Following our previous work [45–48], those quantities are calculated using a combination of *ab initio* and least-squares fitting procedures provided by the Cowan suite of codes [49] and extended in our group. Therefore we provide a theoretical interpretation of Ho even-parity levels, which especially results in the prediction of the widely unmeasured Landé g factors. Because the spectrum of high-Z lanthanide atoms in the ground level is composed of a few strong transitions emerging from a forest of weak ones, the sum-over-state formula is appropriate for calculation of DDPs and C_6 coefficients. It offers the possibility of precisely calculating, with a single set of spectroscopic data, the real and imaginary parts of the scalar, vector, and tensor DDPs in a wide range of wavelengths, especially at 1064 nm, widely used experimentally for trapping purposes.

This article is outlined as follows. We develop our simplified model for the DDP in Sec. II: we first recall useful formulas and, especially, the relationships between scalar, vector, and tensor DDPs and tensor operators (see Sec. II A). Then we calculate the contribution from the levels of a single configuration (see Sec. II B) to the real and imaginary parts of the DDPs, while the two next subsections are devoted to the influence of CI mixing in the DDPs of ground-level lanthanide atoms. Section III deals with the full numerical modeling of the holmium spectrum—energy levels, transition probabilities, polarizabilities, and van der Waals C_6 coefficients (see Secs. III A–III D, respectively). Section IV contains concluding remarks.

II. DYNAMIC DIPOLE POLARIZABILITY: A SIMPLIFIED MODEL

A. Polarizability and tensor operators

For non–spherically symmetric atoms like lanthanides, the ac-Stark shift is a linear combination of three terms, depending on the scalar, vector, and tensor polarizabilities, taken at the angular frequency ω of the oscillating electric field (hereafter denoted the "frequency"). The magnitude of each term is a function of the atomic Zeeman sublevel M and of the electric-field polarization [43]. The scalar $\alpha_{\mathrm{scal}}(\omega)$, vector $\alpha_{\mathrm{vect}}(\omega)$, and tensor polarizabilities $\alpha_{\mathrm{tens}}(\omega)$ can be associated with the coupled polarizabilities $\alpha_k(\omega)$, where $k = 0$, 1, and 2, respectively, are the ranks of the corresponding irreducible tensor [43,50]. Namely,

$$\alpha_{\mathrm{scal}}(\omega) = -\frac{\alpha_0(\omega)}{\sqrt{3(2J+1)}}, \tag{1}$$

$$\alpha_{\mathrm{vect}}(\omega) = \alpha_1(\omega)\sqrt{\frac{2J}{(J+1)(2J+1)}}, \tag{2}$$

$$\alpha_{\mathrm{tens}}(\omega) = \alpha_2(\omega)\sqrt{\frac{2J(2J-1)}{3(J+1)(2J+1)(2J+3)}}. \tag{3}$$

For an atomic level $|\beta J\rangle$, where J is the electronic-angular-momentum quantum number and β stands for all the other quantum numbers, we write the complex polarizability $\alpha_k(\omega)$ by applying the sum-over-state formulation of the second-order time-dependent perturbation theory [51] and assuming complex energies for the intermediate levels $|\beta'' J''\rangle$,

$$\begin{aligned}\alpha_k(\omega) =& \sqrt{2k+1}\sum_{\beta'' J''}(-1)^{J+J''} \\ &\times \begin{Bmatrix} 1 & 1 & k \\ J & J & J'' \end{Bmatrix} |\langle \beta'' J''\|\mathbf{d}\|\beta J\rangle|^2 \\ &\times \left(\frac{(-1)^k}{E_{\beta'' J''} - E_{\beta J} - i\frac{\hbar\gamma_{\beta'' J''}}{2} - \hbar\omega} \right. \\ &\left. + \frac{1}{E_{\beta'' J''} - E_{\beta J} - i\frac{\hbar\gamma_{\beta'' J''}}{2} + \hbar\omega} \right),\end{aligned} \tag{4}$$

where $E_{\beta J}$ ($E_{\beta'' J''}$) are the energies of the levels $|\beta J\rangle$ ($|\beta'' J''\rangle$), $\langle \beta'' J''\|\mathbf{d}\|\beta J\rangle$ is the reduced transition dipole moment between these two levels, $\gamma_{\beta'' J''}$ is the natural line width of the intermediate level $|\beta'' J''\rangle$, and the quantity in curly brackets is a Wigner 6-j symbol [52].

We consider frequencies far from any atomic resonances, i.e., $E_{\beta''J''} - E_{\beta J} \pm \hbar\omega \gg \hbar\gamma_{\beta''J''}/2$, which is relevant for trapping purposes and which greatly simplifies Eq. (4). We separate the real $\mathrm{Re}[\alpha_k(\omega)]$ and imaginary parts $\mathrm{Im}[\alpha_k(\omega)]$,

$$\mathrm{Re}[\alpha_k(\omega)] = 2\sqrt{2k+1}\sum_{\beta''J''}(-1)^{J+J''}\begin{Bmatrix}1 & 1 & k\\ J & J & J''\end{Bmatrix}|\langle\beta''J''\|\mathbf{d}\|\beta J\rangle|^2\frac{(E_{\beta''J''}-E_{\beta J})\delta_{(-1)^k,1}-\hbar\omega\delta_{(-1)^k,-1}}{(E_{\beta''J''}-E_{\beta J})^2-\hbar^2\omega^2}, \tag{5}$$

$$\mathrm{Im}[\alpha_k(\omega)] = \sqrt{2k+1}\sum_{\beta''J''}(-1)^{J+J''}\begin{Bmatrix}1 & 1 & k\\ J & J & J''\end{Bmatrix}\hbar\gamma_{\beta''J''}|\langle\beta''J''\|\mathbf{d}\|\beta J\rangle|^2 \times\frac{[(E_{\beta''J''}-E_{\beta J})^2+\hbar^2\omega^2]\delta_{(-1)^k,1}-2\hbar\omega(E_{\beta''J''}-E_{\beta J})\delta_{(-1)^k,-1}}{[(E_{\beta''J''}-E_{\beta J})^2-\hbar^2\omega^2]^2}, \tag{6}$$

where we have used $A+(-1)^kB = (A+B)\delta_{(-1)^k,1}+(A-B)\delta_{(-1)^k,-1}$. Plugging Eqs. (5) and (6) into Eqs. (1)–(3) and introducing the explicit expressions of 6-j symbols (see Ref. [52], p. 302), we get to the real and imaginary parts of the scalar, vector, and tensor contributions:

$$\mathrm{Re}[\alpha_{\mathrm{scal}}(\omega)] = \frac{2}{3(2J+1)}\sum_{\beta''J''}\frac{(E_{\beta''J''}-E_{\beta J})|\langle\beta''J''\|\mathbf{d}\|\beta J\rangle|^2}{(E_{\beta''J''}-E_{\beta J})^2-\hbar^2\omega^2}, \tag{7}$$

$$\mathrm{Im}[\alpha_{\mathrm{scal}}(\omega)] = \frac{1}{3(2J+1)}\sum_{\beta''J''}\frac{\hbar\gamma_{\beta''J''}[(E_{\beta''J''}-E_{\beta J})^2+\hbar^2\omega^2]|\langle\beta''J''\|\mathbf{d}\|\beta J\rangle|^2}{[(E_{\beta''J''}-E_{\beta J})^2-\hbar^2\omega^2]^2}, \tag{8}$$

$$\mathrm{Re}[\alpha_{\mathrm{vect}}(\omega)] = \sum_{\beta''J''}\frac{J''(J''+1)-J(J+1)-2}{(J+1)(2J+1)}\times\frac{\hbar\omega|\langle\beta''J''\|\mathbf{d}\|\beta J\rangle|^2}{(E_{\beta''J''}-E_{\beta J})^2-\hbar^2\omega^2}, \tag{9}$$

$$\mathrm{Im}[\alpha_{\mathrm{vect}}(\omega)] = \sum_{\beta''J''}\frac{J''(J''+1)-J(J+1)-2}{(J+1)(2J+1)}\times\frac{\hbar^2\omega\gamma_{\beta''J''}(E_{\beta''J''}-E_{\beta J})|\langle\beta''J''\|\mathbf{d}\|\beta J\rangle|^2}{[(E_{\beta''J''}-E_{\beta J})^2-\hbar^2\omega^2]^2}, \tag{10}$$

$$\mathrm{Re}[\alpha_{\mathrm{tens}}(\omega)] = -\sum_{\beta''J''}\frac{3[J''(J''+1)-J(J+1)]^2-9J''(J''+1)+J(J+1)+6}{3(J+1)(2J+1)(2J+3)}\times\frac{(E_{\beta''J''}-E_{\beta J})|\langle\beta''J''\|\mathbf{d}\|\beta J\rangle|^2}{(E_{\beta''J''}-E_{\beta J})^2-\hbar^2\omega^2}, \tag{11}$$

$$\mathrm{Im}[\alpha_{\mathrm{tens}}(\omega)] = -\sum_{\beta''J''}\frac{3[J''(J''+1)-J(J+1)]^2-9J''(J''+1)+J(J+1)+6}{6(J+1)(2J+1)(2J+3)} \times\frac{\hbar\gamma_{\beta''J''}[(E_{\beta''J''}-E_{\beta J})^2+\hbar^2\omega^2]|\langle\beta''J''\|\mathbf{d}\|\beta J\rangle|^2}{[(E_{\beta''J''}-E_{\beta J})^2-\hbar^2\omega^2]^2}. \tag{12}$$

Note that in Eqs. (7), (8), and (11) of Ref. [45], the sign of the vector polarizability is not correct; the error has been fixed in Eqs. (9) and (10) above.

B. Effect of a single intermediate configuration

In this subsection, we assume that the intermediate levels $|\beta''J''\rangle$ appearing in Eq. (4) all belong to the same configuration and that their transition energies $E_{\beta''J''} - E_{\beta J}$ can be replaced by a single effective one. Moreover, we assume that the configurations of the $|\beta J\rangle$ and $|\beta''J''\rangle$ levels differ by the hopping of only one valence electron; in other words, we ignore transitions involving the $4f$ core electrons. This will yield analytical expressions useful for estimating $\alpha_k(\omega)$ and understanding the trapping in some relevant levels, like those belonging to the lowest or the [Xe]$4f^q6s6p$ configurations.

Many levels of lanthanide atoms can be interpreted in the frame of the jj coupling scheme. The electronic core, containing the $4f$ shell, is characterized by its orbital L_c, spin S_c, and total electronic angular momentum J_c. The valence electrons belong, for instance, to the $5d, 6s$, or $6p$ shell. This group of electrons is characterized by their orbital L_v, spin S_v, and total electronic angular momentum J_v. Then J_c and J_v are coupled to give the total electronic angular momentum J of the atomic level. In the present study, we focus on the configurations [Xe]$4f^q.n_1\ell_1n_2\ell_2$ ($q = 10$, 11, and 12 for Dy, Ho, and Er, respectively) with two valence electrons, including, e.g., $4f^q6s^2$ or $4f^q6s6p$; but our results can be extended to configurations with three valence electrons like $4f^{q-1}5d6s^2$ and $4f^{q-1}5d^26s$. The full label of the level is therefore [Xe]$4f^q({}^{2S_c+1}L_{cJ_c}).n_1\ell_1n_2\ell_2({}^{2S_v+1}L_{vJ_v})(J_c,J_v)_J$, and its electronic parity is $(-1)^{q+\ell_1+\ell_2}$. In what follows, we omit the xenon core [Xe] in electronic configurations.

It is noteworthy that the levels of the $4f^q5d6s$ configuration are better described in the jK coupling scheme ${}^{2S_v+1}[K]_J$: J_c is first coupled with L_v to give K, which is itself coupled with S_v to give J. In order to calculate the polarizability of such levels, it is necessary to apply the basis transformation from jj to jK coupling schemes [49]. However, if those levels appear in the sum over $|\beta''J''\rangle$, the jj coupling scheme is sufficient, as all the levels of the $4f^q5d6s$ configuration are assumed to have the same energy (see Sec. II B 2).

1. *Transition dipole moment in jj coupling*

In the electric-dipole (E1) approximation, the transitions with the strongest dipole moments are those for which one

valence electron, say $n_2\ell_2$, is promoted to an orbital $n_2''\ell_2''$ such that $\ell_2'' = \ell_2 \pm 1$. The angular momenta of the atom must also satisfy the selection rules, $L_v'' = L_v$ or $L_v \pm 1$, $S_v'' = S_v$, $J_v'' = J_v$ or $J_v \pm 1$, and $J'' = J$ or $J \pm 1$, excluding transitions between couples of angular momenta (0,0), whereas the quantum numbers of the core are not modified ($L_c'' = L_c$, $S_c'' = S_c$, and $J_c'' = J_c$). In the frame of the jj coupling scheme, we can express the reduced transition dipole moment between the levels $|\beta J\rangle$ and $|\beta'' J''\rangle$ as a function of the monoelectronic transition dipole moment (MTDM) $\langle n_2''\ell_2''|\hat{r}|n_2\ell_2\rangle$ expressed as the matrix element of the monoelectronic $\hat{r}$ operator. We apply the following successive steps [49].

By writing atomic levels as the lists of quantum numbers $|n_1\ell_1 n_2\ell_2 L_v S_v J_v J_c J\rangle$ (and similarly for double-primed quantum numbers), we start working with (J_c, J_v, J),

$$\begin{aligned}&|\langle n_1\ell_1 n_2''\ell_2'' L_v'' S_v J_v'' J_c J''\|\mathbf{d}\|n_1\ell_1 n_2\ell_2 L_v S_v J_v J_c J\rangle|^2\\ &\quad= (2J+1)(2J''+1)\begin{Bmatrix} J_v & J_c & J\\ J'' & 1 & J_v''\end{Bmatrix}^2\\ &\qquad\times |\langle n_1\ell_1 n_2''\ell_2'' L_v'' S_v J_v''\|\mathbf{d}\|n_1\ell_1 n_2\ell_2 L_v S_v J_v\rangle|^2. \qquad (13)\end{aligned}$$

Then we go one step further, with (L_v, S_v, J_v),

$$\begin{aligned}&|\langle n_1\ell_1 n_2''\ell_2'' L_v'' S_v J_v''\|\mathbf{d}\|n_1\ell_1 n_2\ell_2 L_v S_v J_v\rangle|^2\\ &\quad= (2J_v+1)(2J_v''+1)\begin{Bmatrix} L_v & S_v & J_v\\ J_v'' & 1 & L_v''\end{Bmatrix}^2\\ &\qquad\times |\langle n_1\ell_1 n_2''\ell_2'' L_v''\|\mathbf{d}\|n_1\ell_1 n_2\ell_2 L_v\rangle|^2, \qquad (14)\end{aligned}$$

and with (n_1, ℓ_1, n_2, ℓ_2, L_v),

$$\begin{aligned}&|\langle n_1\ell_1 n_2''\ell_2'' L_v''\|\mathbf{d}\|n_1\ell_1 n_2\ell_2 L_v\rangle|^2\\ &\quad= (1+\delta_{n_1n_2}\delta_{\ell_1\ell_2})(1+\delta_{n_1n_2''}\delta_{\ell_1\ell_2''})(2L_v+1)\\ &\qquad\times (2L_v''+1)\begin{Bmatrix} \ell_2 & \ell_1 & L_v\\ L_v'' & 1 & \ell_2''\end{Bmatrix}^2 |\langle n_2''\ell_2''\|\mathbf{d}\|n_2\ell_2\rangle|^2, \qquad (15)\end{aligned}$$

where the δ's are Kronecker symbols, which bring a factor of 2 for equivalent electrons $(n_1\ell_1) = (n_2\ell_2)$ or $(n_1\ell_1) = (n_2''\ell_2'')$. Finally,

$$\begin{aligned}|\langle n_2''\ell_2''\|\mathbf{d}\|n_2\ell_2\rangle|^2 &= e^2 r^2_{n_2\ell_2,n_2''\ell_2''}(2\ell_2+1)\\ &\quad\times (2\ell_2''+1)\begin{pmatrix} \ell_2'' & 1 & \ell_2\\ 0 & 0 & 0\end{pmatrix}^2, \qquad (16)\end{aligned}$$

where (:::) is a Wigner 3-j symbol, e is the absolute value of the electronic charge, and $r_{n_2\ell_2,n_2''\ell_2''} = r_{n_2''\ell_2'',n_2\ell_2} \equiv \langle n_2''\ell_2''|\hat{r}|n_2\ell_2\rangle$.

2. *Real part of the polarizability*

We assume that the polarizability $\alpha_k(\omega)$ of level $|\beta J\rangle$ [see Eq. (4)] involves transitions towards levels $|\beta'' J''\rangle$ belonging to configurations of the kind $4f^q.n_1\ell_1.n_2''\ell_2''$. By separating the contributions of those configurations, we can write

$$\alpha_k(\omega) = \sum_{n_2''\ell_2''} \alpha_k^{n_2''\ell_2''}(\omega), \qquad (17)$$

which relies on two main hypotheses: (i) Transitions to levels of configurations in which one core electron is excited, e.g., $4f^{q-1}.5d.n_1\ell_1.n_2\ell_2$, are excluded, as they are often significantly weaker. (ii) Configuration interaction is totally neglected, both between different configurations of the kind $4f^q.n_1\ell_1.n_2''\ell_2''$ and with those of the kind $4f^{q-1}.n''\ell''.n_1\ell_1.n_2\ell_2$. The effect of CI is addressed in the next subsection.

The central assumption of this work is that the energy differences implying the levels of a given configuration can be replaced with a single effective energy $\hbar\omega_{n_2''\ell_2''}$:

$$E_{\beta'' J''} - E_{\beta J} \approx \hbar\omega_{n_2''\ell_2''}. \qquad (18)$$

The validity of this assumption depends on the frequency ω at which the DDPs are calculated, which should not "fall" into the levels of the $4f^q.n_1\ell_1.n_2''\ell_2''$ configuration. If we denote $\min(E_{\beta'' J''})$ and $\max(E_{\beta'' J''})$ their lowest and highest energies, Eq. (18) is not applicable for

$$\min(E_{\beta'' J''}) - E_{\beta J} \lesssim \bar{\omega} \lesssim \max(E_{\beta'' J''}) - E_{\beta J}, \qquad (19)$$

where $\bar{\omega} = \pm\omega$ for $E_{\beta'' J''} > E_{\beta J}$ and $E_{\beta'' J''} < E_{\beta J}$, respectively. For ground-level Ho, the excluded frequencies, which correspond to the energies of the $4f^{11}(^4I^o_{15/2}).6s6p(^1P^o_1)(15/2,1)$ manifold, roughly range from 23 000 to 24 000 cm^{-1}.

Consequently, the sum in Eq. (4) is restricted to the quantum numbers L_v'', $'J_v''$, and J'' allowed by electric-dipole transitions. (For configurations with at least one s electron, there is obviously only one possible L_v value.) Inserting Eq. (17) into Eq. (5), we can extract the real part:

$$\begin{aligned}\mathrm{Re}\big[\alpha_k^{n_2''\ell_2''}(\omega)\big] &= \frac{2\big(\omega_{n_2''\ell_2''}\,\delta_{(-1)^k,1} - \omega\,\delta_{(-1)^k,-1}\big)}{\hbar\big(\omega^2_{n_2''\ell_2''} - \omega^2\big)}\sqrt{2k+1}\sum_{L_v''J_v''J''}(-1)^{J+J''}\begin{Bmatrix} 1 & 1 & k\\ J & J & J''\end{Bmatrix}\\ &\quad\times |\langle n_1\ell_1 n_2''\ell_2'' L_v'' S_v J_v'' J_c J''\|\mathbf{d}\|n_1\ell_1 n_2\ell_2 L_v S_v J_v J_c J\rangle|^2. \qquad (20)\end{aligned}$$

Using Eq. (13), we obtain

$$\begin{aligned}\mathrm{Re}\big[\alpha_k^{n_2''\ell_2''}(\omega)\big] &= \frac{2\big(\omega_{n_2''\ell_2''}\,\delta_{(-1)^k,1} - \omega\,\delta_{(-1)^k,-1}\big)}{\hbar\big(\omega^2_{n_2''\ell_2''} - \omega^2\big)}\sqrt{2k+1}\sum_{L_v''J_v''J''}(-1)^{J+J''}\begin{Bmatrix} 1 & 1 & k\\ J & J & J''\end{Bmatrix}\\ &\quad\times (2J+1)(2J''+1)\begin{Bmatrix} J_v & J_c & J\\ J'' & 1 & J_v''\end{Bmatrix}^2 |\langle n_1\ell_1 n_2''\ell_2'' L_v'' S_v J_v''\|\mathbf{d}\|n_1\ell_1 n_2\ell_2 L_v S_v J_v\rangle|^2. \qquad (21)\end{aligned}$$

To calculate this expression, we note that the quantum number J'' only appears in angular terms, so that we use the identity (see Ref. [52], p. 305)

$$\sum_X (-1)^{R+X}(2X+1)\begin{Bmatrix} a & b & p \\ c & d & X \end{Bmatrix}\begin{Bmatrix} c & d & q \\ e & f & X \end{Bmatrix}\begin{Bmatrix} e & f & r \\ b & a & X \end{Bmatrix} = \begin{Bmatrix} p & q & r \\ e & a & d \end{Bmatrix}\begin{Bmatrix} p & q & r \\ f & b & c \end{Bmatrix}, \tag{22}$$

with $R = a+b+c+d+e+f+p+q+r$, as well as the invariance properties of Wigner 6-j symbols with respect to line and column permutations. Applying Eq. (22) with $a = d = 1$, $b = c = J$, $e = J''_v$, $f = J_c$, $p = k$, and $q = r = J_v$, we can get rid of J'' in Eq. (21):

$$\begin{aligned}\mathrm{Re}\big[\alpha_k^{n''_2\ell''_2}(\omega)\big] = {}& \frac{2\big(\omega_{n''_2\ell''_2}\,\delta_{(-1)^k,1} - \omega\,\delta_{(-1)^k,-1}\big)}{\hbar\big(\omega^2_{n''_2\ell''_2} - \omega^2\big)}\sqrt{2k+1}\sum_{L''_vJ''_v}(-1)^{J_c+2J_v+J''_v+J+k} \\ & \times (2J+1)\begin{Bmatrix} 1 & 1 & k \\ J_v & J_v & J''_v \end{Bmatrix}\begin{Bmatrix} J_v & J_c & J \\ J & k & J_v \end{Bmatrix}|\langle n_1\ell_1n''_2\ell''_2L''_vS_vJ''_v\|\mathbf{d}\|n_1\ell_1n_2\ell_2L_vS_vJ_v\rangle|^2 .\end{aligned} \tag{23}$$

At this point, it is the following fact is noteworthy [53]. The definitions of the coupled polarizabilities $\alpha_k(\omega)$ and $\alpha_k^{n''_2\ell''_2}(\omega)$, given, respectively, by Eqs. (4) and (17), are such that they can be written as the reduced matrix elements of the operators $\hat{\alpha}_k(\omega)$ and $\hat{\alpha}_k^{n''_2\ell''_2}(\omega)$, which are tensors of rank k. In particular, one can resort to the Wigner-Eckart theorem [52] to calculate the coupled polarizability of a level $|\beta JM\rangle$, namely, $\langle\beta JM|\hat{\alpha}_k(\omega)|\beta JM\rangle = \langle\beta J\|\hat{\alpha}_k(\omega)\|\beta J\rangle \times C^{JM}_{JMk0}/\sqrt{2J+1}$, with C^{JM}_{JMk0} a Clebsh-Gordan coefficient [and similarly for $\hat{\alpha}_k^{n''_2\ell''_2}(\omega)$]. One can also apply the transformation of tensor operators regarding angular-momentum basis sets; in this respect, Eq. (23) can be seen as such a transformation,

$$\begin{aligned}&\langle n_1\ell_1n_2\ell_2L_vS_vJ_vJ_cJ\|\mathrm{Re}\big[\hat{\alpha}_k^{n''_2\ell''_2}(\omega)\big]\|n_1\ell_1n_2\ell_2L_vS_vJ_vJ_cJ\rangle \\ &\quad = (-1)^{J_c+J_v+k+J}(2J+1)\begin{Bmatrix} J_v & J_c & J \\ J & k & J_v \end{Bmatrix}\langle n_1\ell_1n_2\ell_2L_vS_vJ_v\|\mathrm{Re}\big[\hat{\alpha}_k^{n''_2\ell''_2}(\omega)\big]\|n_1\ell_1n_2\ell_2L_vS_vJ_v\rangle ,\end{aligned} \tag{24}$$

where

$$\begin{aligned}&\langle n_1\ell_1n_2\ell_2L_vS_vJ_v\|\mathrm{Re}\big[\hat{\alpha}_k^{n''_2\ell''_2}(\omega)\big]\|n_1\ell_1n_2\ell_2L_vS_vJ_v\rangle \\ &\quad = \frac{2\big(\omega_{n''_2\ell''_2}\,\delta_{(-1)^k,1} - \omega\,\delta_{(-1)^k,-1}\big)}{\hbar\big(\omega^2_{n''_2\ell''_2} - \omega^2\big)}\sqrt{2k+1}\sum_{J''_vL''_v}(-1)^{J_v+J''_v}\begin{Bmatrix} 1 & 1 & k \\ J_v & J_v & J''_v \end{Bmatrix}|\langle n_1\ell_1n''_2\ell''_2L''_vS_vJ''_v\|\mathbf{d}\|n_1\ell_1n_2\ell_2L_vS_vJ_v\rangle|^2 .\end{aligned} \tag{25}$$

Returning to our main purpose, we apply Eq. (22) twice more: first, with Eq. (14) to express the sum over J''_v and, second, with Eq. (15) to express the sum over L''_v. Doing so, we get to the final expression,

$$\begin{aligned}\mathrm{Re}\big[\alpha_k^{n''_2\ell''_2}(\omega)\big] = {}& \frac{2\sqrt{2k+1}}{\hbar}\times\frac{\omega_{n''_2\ell''_2}\,\delta_{(-1)^k,1} - \omega\,\delta_{(-1)^k,-1}}{\omega^2_{n''_2\ell''_2} - \omega^2}(1+\delta_{n_1n_2}\delta_{\ell_1\ell_2}) \\ & \times(1+\delta_{n_1n''_2}\delta_{\ell_1\ell''_2})(-1)^{J+J_c-S_v+\ell_1+\ell''_2+k}(2J+1)(2J_v+1)(2L_v+1)(2\ell_2+1)(2\ell''_2+1) \\ & \times\begin{Bmatrix} J_v & J_c & J \\ J & k & J_v \end{Bmatrix}\begin{Bmatrix} L_v & S_v & J_v \\ J_v & k & L_v \end{Bmatrix}\begin{Bmatrix} \ell_2 & \ell_1 & L_v \\ L_v & k & \ell_2 \end{Bmatrix}\begin{Bmatrix} 1 & 1 & k \\ \ell_2 & \ell_2 & \ell''_2 \end{Bmatrix}\begin{pmatrix} \ell''_2 & 1 & \ell_2 \\ 0 & 0 & 0 \end{pmatrix}^2 e^2r^2_{n_2\ell_2,n''_2\ell''_2},\end{aligned} \tag{26}$$

which depends on two effective parameters: the transition frequency $\omega_{n''_2\ell''_2}$ and the MTDM $-er_{n_2\ell_2,n''_2\ell''_2}$.

The rest of Eq. (26) consists of very insightful angular terms. In particular, the 6-j symbols indicate that, if one of the quantum numbers J, J_v, or L_v is equal to 0, then the vector and tensor polarizabilities, proportional to $\mathrm{Re}[\alpha_{k=1}^{n''_2\ell''_2}(\omega)]$ and $\mathrm{Re}[\alpha_{k=2}^{n''_2\ell''_2}(\omega)]$), respectively, vanish. This is, for instance, the case for lanthanides at their ground level, which is characterized by $L_v = J_v = 0$. In our full numerical calculation of the polarizability [45,46], we have shown that indeed the vector and tensor contributions are much weaker than the scalar one. Equation (26) tends to confirm that those weak contributions come from transitions in which one $4f$ electron is excited. Such conclusions are also valid for any level belonging to the lowest configuration $4f^q6s^2$, as shown in our previous articles (see Ref. [46] and Sec. III C here).

3. *Imaginary part of the polarizability*

For the imaginary part to be relevant, we consider a metastable level $|\beta J\rangle$, i.e., whose natural line width $\gamma_{\beta J}$ is negligible compared to the photon-scattering rate induced by the electromagnetic field [44,45]. In practice, this may concern excited levels of the lowest configuration $4f^q6s^2$ or the levels $4f^q(^{2S_c+1}L_{cJ_c}).6s6p(^3P_2)\,(J_c,2)_{J_c+2}$, which have no decay channel in the E1 approximation [except for level $(6,2)^o_8$ of Er] [54].

As Eq. (6) shows, the imaginary part of the polarizability involves the natural line width of intermediate levels $|\beta'' J''\rangle$,

$$\gamma_{\beta'' J''} = \sum_{\tilde{\beta}\tilde{J},\, E_{\tilde{\beta}\tilde{J}} < E_{\beta'' J''}} A_{\beta'' J'', \tilde{\beta}\tilde{J}} = \frac{\sum_{\tilde{\beta}\tilde{J}} (E_{\beta'' J''} - E_{\tilde{\beta}\tilde{J}})^3 |\langle \beta'' J'' \| \mathbf{d} \| \tilde{\beta}\tilde{J}\rangle|^2}{3\pi\epsilon_0 \hbar^4 c^3 (2J''+1)}, \tag{27}$$

where $A_{\beta'' J'', \tilde{\beta}\tilde{J}}$ is the transition probability characterizing the spontaneous emission from level $|\beta'' J''\rangle$ to level $|\tilde{\beta}\tilde{J}\rangle$. We focus on the influence of the $\beta'' J''$ levels belonging to the configuration $4f^q.n_1\ell_1.n_2''\ell_2''$. In addition, we assume that the latter levels only decay towards levels $|\tilde{\beta}\tilde{J}\rangle$ belonging to the configuration $4f^q.n_1\ell_1.n_2\ell_2$. Therefore the sum in Eq. (27) runs over the quantum numbers $\tilde{J}$, $\tilde{J}_v$, and $\tilde{L}_v$. If we express the squared reduced transition dipole moment as in Eq. (13), Eq. (27) becomes

$$\gamma_{L_v'' J_v'' J''} = \frac{\omega^3_{n_2''\ell_2''}}{3\pi\epsilon_0\hbar c^3} \sum_{\tilde{L}_v \tilde{J}_v \tilde{J}} (2\tilde{J}+1) \begin{Bmatrix} \tilde{J}_v & J_c & \tilde{J} \\ J'' & 1 & J_v'' \end{Bmatrix}^2 \times |\langle n_1\ell_1 n_2''\ell_2'' L_v'' S_v J_v'' \| \mathbf{d} \| n_1\ell_1 n_2\ell_2 \tilde{L}_v S_v \tilde{J}_v\rangle|^2. \tag{28}$$

Since $\tilde{J}$ only appears in angular factors, the sum over $\tilde{J}$ reduces to the orthogonalization relations of 6-j symbols,

$$\sum_{\tilde{J}} (2\tilde{J}+1) \begin{Bmatrix} \tilde{J}_v & J_c & \tilde{J} \\ J'' & 1 & J_v'' \end{Bmatrix}^2 = \frac{1}{2J_v''+1}. \tag{29}$$

Using Eqs. (14) and (15) for the transition dipole moment, we can calculate the sums over $\tilde{J}_v$ and $\tilde{L}_v$ in a similar way, and finally, we get to the expression [see also Eq. (16)]

$$\gamma_{L_v'' J_v'' J''} = \frac{\omega^3_{n_2''\ell_2''} e^2 r^2_{n_2\ell_2, n_2''\ell_2''}}{3\pi\epsilon_0\hbar c^3} (2\ell_2+1) \begin{pmatrix} \ell_2'' & 1 & \ell_2 \\ 0 & 0 & 0 \end{pmatrix}^2 \times \left(1 + \delta_{n_1 n_2}\delta_{\ell_1\ell_2}\right)\left(1 + \delta_{n_1 n_2''}\delta_{\ell_1\ell_2''}\right). \tag{30}$$

Strikingly, the natural line width of the intermediate levels does not depend on L_v'', J_v'', or J''; it is identical for all the levels of the $4f^q.n_1\ell_1.n_2''\ell_2''$ configuration. In calculating $\mathrm{Im}[\alpha_k^{n_2''\ell_2''}(\omega)]$, we can factorize $\gamma_{L_v'' J_v'' J''}$ out of the sum over L_v'', J_v'', and J'', and so steps similar [see Eqs. (21)–(26)] to those for the real part can be applied, which leads to the final expression

$$\begin{aligned} \mathrm{Im}\left[\alpha_k^{n_2''\ell_2''}(\omega)\right] = {} & \frac{\omega^3_{n_2''\ell_2''}\sqrt{2k+1}}{3\pi\epsilon_0\hbar^2 c^3} \times \frac{\left(\omega^2_{n_2''\ell_2''} + \omega^2\right)\delta_{(-1)^k,1} - 2\omega\omega_{n_2''\ell_2''}\,\delta_{(-1)^k,-1}}{\left(\omega^2_{n_2''\ell_2''} - \omega^2\right)^2} \left(1 + \delta_{n_1 n_2}\delta_{\ell_1\ell_2}\right)^2 \left(1 + \delta_{n_1 n_2''}\delta_{\ell_1\ell_2''}\right)^2 \\ & \times (-1)^{J+J_c-S_v+\ell_1+\ell_2''+k} (2J+1)(2J_v+1)(2L_v+1)(2\ell_2+1)^2(2\ell_2''+1) \\ & \times \begin{Bmatrix} J_v & J_c & J \\ J & k & J_v \end{Bmatrix} \begin{Bmatrix} L_v & S_v & J_v \\ J_v & k & L_v \end{Bmatrix} \begin{Bmatrix} \ell_2 & \ell_1 & L_v \\ L_v & k & \ell_2 \end{Bmatrix} \begin{Bmatrix} 1 & 1 & k \\ \ell_2 & \ell_2 & \ell_2'' \end{Bmatrix} \begin{pmatrix} \ell_2'' & 1 & \ell_2 \\ 0 & 0 & 0 \end{pmatrix}^4 e^4 r^4_{n_2\ell_2, n_2''\ell_2''}. \end{aligned} \tag{31}$$

Therefore, similarly to the real part, the imaginary part of the polarizability depends on the effective frequency $\omega_{n_2''\ell_2''}$ and the monoelectronic transition dipole moment $-er_{n_2\ell_2, n_2''\ell_2''}$ between the two configurations and on some angular factors.

Again, those angular factors show that, if one of the quantum numbers J, J_v, or L_v is equal to 0, then the vector and tensor polarizabilities are equal to 0. For lanthanide atoms in the ground level, our simplified model predicts that both the real and the imaginary parts of the vector and tensor DDPs vanish [see, respectively, Eqs. (26) and (31)]. For the real part, that prediction agrees with our full numerical calculation [45,46] (see also Sec. III C), but for the imaginary part it does not. To explain this contradiction, we note that the vector-to-scalar and tensor-to-scalar ratios are significantly higher for Er than for Dy and Ho. In addition, Er is the only atom among the three for which we modeled the excited levels including the configurations $4f^{11}5d6s^2$, $4f^{11}5d^26s$, and $4f^{12}6s6p$, and so we expect to have a better description of CI mixing for it. This tends to prove that CI plays an important role in the imaginary part of the DDPs. That is why, in the next subsection, we improve our model by taking into account CIs among excited levels.

C. Effect of configuration interaction

We focus on the polarizability of the ground level of lanthanides, denoted $|\beta J\rangle \equiv |0J\rangle$ and characterized by $L_v = S_v = 0$ and $J = J_c$. According to Eqs. (26) and (31), there are three excited levels, denoted $|1J''\rangle$ for $J'' = J$ and $J \pm 1$, which contribute to the polarizability; they are characterized by $L_v'' = J_v'' = 1$. In this section, we consider that these levels can be mixed by CI to other levels $|mJ''\rangle$ belonging to other configurations. Therefore the eigenvector of the excited levels $|\beta'' J''\rangle$ can be expanded as

$$|\beta'' J''\rangle = \sum_{m \geqslant 1} c^{(J'')}_{\beta'' m} |mJ''\rangle, \tag{32}$$

where $|mJ''\rangle$ are henceforth called basis states. Furthermore, we assume that state $|1J''\rangle$ is the only one contributing to the transition dipole moment $\langle 0J \| \mathbf{d} \| \beta'' J''\rangle$. This is exactly valid for basis states of the $4f^{q-1}5d^26s$ configuration and approximately valid for states of the $4f^{q-1}5d6s^2$ configuration, as the latter contribute significantly less than states of the $4f^q6s6p$ configuration.

In this case the squared transition dipole moment reads

$$|\langle \beta'' J'' \| \mathbf{d} \| 0J\rangle|^2 = \left|c^{(J'')}_{\beta'',1}\right|^2 |\langle 1J'' \| \mathbf{d} \| 0J\rangle|^2 = \tfrac{2}{3} w^{(J'')}_{\beta'',1} (2J''+1) r^2_{6s6p}, \tag{33}$$

where, in the second line, we have expressed $|\langle 1J'' \| \mathbf{d} \| 0J\rangle|^2$ using Eqs. (13)–(16) and the explicit forms of the 3-j and

6-j symbols. In Eq. (33) we introduced the weights $w^{(J'')}_{\beta'',1} = |c^{(J'')}_{\beta'',1}|^2$ of the basis states $|1J''\rangle$ in levels $|\beta''J''\rangle$, which satisfy the normalization conditions

$$\sum_{m\geqslant 1} w^{(J'')}_{\beta''m} = \sum_{\beta''} w^{(J'')}_{\beta''m} = 1 \tag{34}$$

for each J'' separately.

Turning to the polarizability, we find that the real part is

$$\begin{aligned}\mathrm{Re}\big[\alpha^{6p}_k(\omega)\big] &= \frac{4e^2 r^2_{6s6p}\sqrt{2k+1}}{3\hbar}\,\frac{\omega_{6p}\,\delta_{(-1)^k,1} - \omega\,\delta_{(-1)^k,-1}}{\omega^2_{6p}-\omega^2}\\ &\times \sum_{J''}(-1)^{J+J''}(2J''+1)\begin{Bmatrix}1 & 1 & k\\ J & J & J''\end{Bmatrix}\sum_{\beta''} w^{(J'')}_{\beta'',1}\\ &= -\frac{4e^2 r^2_{6s6p}\omega_{6p}\,\delta_{k0}}{\hbar\big(\omega^2_{6p}-\omega^2\big)}\sqrt{\frac{2J+1}{3}},\end{aligned} \tag{35}$$

where the sums over β'' and J'' are calculated using, respectively, Eq. (34) and (see Ref. [52], p. 305)

$$\begin{aligned}&\sum_X (-1)^{a+b+X}(2X+1)\begin{Bmatrix}a & a & c\\ b & b & X\end{Bmatrix}\\ &\quad = \delta_{c0}\sqrt{(2a+1)(2b+1)},\end{aligned} \tag{36}$$

with $a = 1, b = J, c = k$, and $X = J''$. Equation (35) shows that the vector and tensor polarizabilities vanish for lanthanides in the ground level (or in any level of the electronic configuration $4f^q6s^2$), whatever the CI mixing in the excited levels; the only contribution is thus the scalar one, $\mathrm{Re}[\alpha_{\mathrm{scal}}(\omega)] = 4e^2r^2_{6s6p}\omega_{6p}/3\hbar(\omega^2_{6p}-\omega^2)$. In this respect the inclusion of CI in our model does not modify the conclusions in the single-configuration case [see Eq. (26)]. This confirms that, as shown in our full numerical calculations in Sec. III, the vector and tensor contributions arise from the $4f$-$5d$ transitions between the configurations $4f^q6s^2$ and $4f^{q-1}5d6s^2$, depending on r_{4f5d}. By contrast, in Eq. (35), even if levels $|\beta''J''\rangle$ may contain some $4f^{q-1}5d6s^2$ character, the contribution of the $4f^q6s^2$-$4f^q6s6p$ transition is the only one considered in $|\langle\beta''J''\|\mathbf{d}\|0J\rangle|^2$ [see Eq. (33)].

In order to calculate the imaginary part of the polarizability, we recall that the excited level $|1J''\rangle$ can only decay toward the ground level $|0J\rangle$. Therefore $\mathrm{Im}[\alpha^{6p}_k(\omega)]$ reads

$$\begin{aligned}\mathrm{Im}\big[\alpha^{6p}_k(\omega)\big] &= \frac{\big(\omega^2_{6p}+\omega^2\big)\,\delta_{(-1)^k,1} - 2\omega\omega_{6p}\,\delta_{(-1)^k,-1}}{\big(\omega^2_{6p}-\omega^2\big)^2}\\ &\times \frac{\omega^3_{6p}\sqrt{2k+1}}{3\pi\epsilon_0\hbar^2c^3}\sum_{J''}(-1)^{J+J''}\begin{Bmatrix}1 & 1 & k\\ J & J & J''\end{Bmatrix}\\ &\times \sum_{\beta''}\frac{1}{2J''+1}|\langle\beta''J''\|\mathbf{d}\|0J\rangle|^4\\ &= \frac{\big(\omega^2_{6p}+\omega^2\big)\,\delta_{(-1)^k,1} - 2\omega\omega_{6p}\,\delta_{(-1)^k,-1}}{\big(\omega^2_{6p}-\omega^2\big)^2}\\ &\times \frac{4\omega^3_{6p}r^4_{6s6p}\sqrt{2k+1}}{27\pi\epsilon_0\hbar^2c^3}\sum_{J''}(-1)^{J+J''}(2J''+1)\\ &\times \begin{Bmatrix}1 & 1 & k\\ J & J & J''\end{Bmatrix}\sum_{\beta''}\big(w^{(J'')}_{\beta'',1}\big)^2,\end{aligned} \tag{37}$$

where we have taken the square of Eq. (33).

Equation (37) is a key result of this work. Contrary to the real part given by Eq. (35), the sum over β'' cannot be simplified in the imaginary part of the polarizability, as it involves the squared weights of the $|1J''\rangle$ basis vectors in the excited levels $|\beta''J''\rangle$. In this respect, we can say that the imaginary part of the polarizability is more sensitive to the details of the atomic structure than the real part.

In particular, taking the square of Eq. (34), we find that

$$\begin{aligned}\sum_{\beta''}\Big(w^{(J'')}_{\beta''m}\Big)^2 &= \Bigg(\sum_{\beta''} w^{(J'')}_{\beta''m}\Bigg)^2 - 2\sum_{\substack{\beta''_1\beta''_2\\ \beta''_1<\beta''_2}} w^{(J'')}_{\beta''_1m}w^{(J'')}_{\beta''_2m}\\ &= 1 - 2\sum_{\substack{\beta''_1\beta''_2\\ \beta''_1<\beta''_2}} w^{(J'')}_{\beta''_1m}w^{(J'')}_{\beta''_2m} \leqslant 1,\end{aligned} \tag{38}$$

where $\beta''_1 < \beta''_2$ means $E_{\beta''_1J''} < E_{\beta''_2J''}$, to avoid double-counting. The inequality comes from the fact that $w^{(J'')}_{\beta''m} \geqslant 0, \forall\, m, \beta'', J''$. The limit for which Eq. (38) is unity corresponds to the case where one weight is unity and all the others are 0, i.e., there is no CI. In this particular case, the sums over β'' and J'' in Eq. (37) can be simplified,

$$\mathrm{Im}\big[\alpha^{6p}_k(\omega)\big] = -\frac{4\omega^3_{6p}\big(\omega^2_{6p}+\omega^2\big)e^4r^4_{6s6p}\delta_{k0}}{9\pi\epsilon_0\hbar^2c^3\big(\omega^2_{6p}-\omega^2\big)^2}\sqrt{\frac{2J+1}{3}}, \tag{39}$$

and so $\mathrm{Im}\alpha^{6p}_{\mathrm{scal}}(\omega)] = 4\omega^3_{6p}(\omega^2_{6p}+\omega^2)e^4r^4_{6s6p}/27\pi\epsilon_0\hbar^2c^3(\omega^2_{6p}-\omega^2)^2$, which can also be obtained from Eq. (31). By comparing Eqs. (37)–(39), we find that CI has two effects:

(i) It tends to reduce the scalar contribution $\mathrm{Im}[\alpha^{6p}_0(\omega)]$. Indeed in the limit of strong CI mixing, when N basis states $|mJ''\rangle$ ($m = 1$ to N) are equally spread over N excited levels $|\beta''J''\rangle$, which means that $w^{(J'')}_{\beta''m} = 1/N$ for all J'', then Eq. (38) is $1/N$, and Eq. (39) is divided by N.

(ii) It tends to enhance the vector $\mathrm{Im}[\alpha^{6p}_1(\omega)]$ and tensor $\mathrm{Im}[\alpha^{6p}_2(\omega)]$ contributions, because for arbitrary weights (different from 0, 1, and $1/N$), the three J'' terms in Eq. (37) do not exactly compensate each other.

The weights $w^{(J'')}_{\beta''m}$ associated with the eigenvectors of excited energy levels are therefore crucial for calculation of the imaginary part of the polarizability. In our previous work on erbium [45], we described the odd-parity levels with the configurations $4f^{12}6s6p$, $4f^{11}5d6s^2$, and $4f^{11}5d^26s$, which is likely to yield a reliable calculation of the weights $w^{(J'')}_{\beta'',1}$, which play an important part in the polarizability. By contrast, we did not consider the configurations $4f^{q-1}5d^26s$ for Dy ($q = 10$) and Ho ($q = 11$), because of the large number of levels belonging to these configurations. Since some of the weights $w^{(J'')}_{\beta''m}$ are not correct, our computed imaginary polarizabilities must be taken with caution. The relatively low

ratio of the vector and tensor contributions with respect to the scalar one, observed in Ref. [46] and Sec. III C, may be due to the lack of CI in our eigenvectors. In the next section, we present a method to estimate the weights $w^{(J'')}_{\beta'',1}$ from experimental values of the transition probabilities.

D. Estimate of configuration-interaction mixing

We consider transition probabilities $A_{\beta''J'',J0}$, characterizing the spontaneous emissions from level $|\beta''J''\rangle$ towards the ground level $|0J\rangle$, which are given by Eq. (27) with $|\tilde{\beta}\tilde{J}\rangle = |0J\rangle$. Assuming that the transition is due to the coupling between basis states $|1J''\rangle$ and $|0J\rangle$, we obtain that the squared transition dipole moment is proportional to $w^{(J'')}_{\beta'',1}$ [see Eq. (33)], and so the Einstein coefficient is proportional to $A_{\beta''J'',0J} \propto w^{(J'')}_{\beta'',1} \times (E_{\beta''J''} - E_{0J})^3$. Supposing all transition energies approximately equal, i.e., $E_{\beta''J''} - E_{0J} \approx \hbar\omega_{6p}$, yields that the sum of the transition probabilities for a given J and J'' is a J- and J''-independent constant,

$$\sum_{\beta''} A_{\beta''J'',0J} \approx \frac{2\omega_{6p}^3 e^2 r_{6s,6p}^2}{3\pi\epsilon_0\hbar c^3}. \tag{40}$$

Therefore, knowing the transition energies and transition probabilities, we can express the weight $w^{(J'')}_{\beta'',1}$ as

$$w^{(J'')}_{\beta'',1} = \frac{\frac{A_{\beta''J'',0J}}{(E_{\beta''J''}-E_{0J})^3}}{\sum_{\beta^*}\frac{A_{\beta^*J'',0J}}{(E_{\beta^*J''}-E_{0J})^3}}, \tag{41}$$

where the terms $(E_{\beta''J''} - E_{0J})$ and $(E_{\beta^*J''} - E_{0J})$ have been explicitly written, in order to get a better estimate of $w^{(J'')}_{\beta'',1}$, even though they could be approximated by $\hbar\omega_{6p}$.

In practice, Lawler and Den Artog's group performed extensive measurements of transition probabilities, especially in dysprosium [55], holmium [56], erbium [57], and thulium [58]. The spectrum of the ground level is composed of a forest of weak transitions from which emerge a few strong transitions with similar transition energies. The number of strong lines (say with $A_{\beta''J'',0J} > 10^7\ \mathrm{s}^{-1}$) increases with increasing atomic number. When calculating the sum of Einstein coefficients for separated J'' [see Eq. (40)], one usually finds 2.1 to $2.4 \times 10^8\ \mathrm{s}^{-1}$. Among these transitions, some are certainly due not to $6s$-$6p$ but, rather, to $4f$-$5d$ excitation; however, they are so weak that they will not affect the calculation of $w^{(J'')}_{\beta'',1}$ with Eq. (41).

In the case of erbium, we modeled the erbium spectrum including configurations $4f^{12}6s6p$, $4f^{11}5d6s^2$, and $4f^{11}5d^26s$ [45], while we did not include either $4f^95d^26s$ for dysprosium [46] or $4f^{10}5d^26s$ for holmium (see Sec. III). So for erbium, the "experimental" weights, given by Eq. (41), can be compared with the "theoretical" ones, which we can extract from our modeling of the spectrum [45]. The results are listed in Table I for the odd-parity levels giving the strongest transitions (with probabilities higher than $10^7\ \mathrm{s}^{-1}$) towards the ground level $4f^{12}6s^2\,{}^3H_6$. In Table I we also compare the energies and transition probabilities. As discussed in Ref. [45], the agreementfor the energy is very good. As for the transition probabilities, the overall agreement is satisfactory, even if the theoretical transition probabilities and weights are globally lower than the experimental ones. For a given level $|\beta''J''\rangle$, the discrepancies in $A_{\beta''J'',0J}$ and for $w^{(J'')}_{\beta'',1}$ are actually similar. This confirms our assumption that the strongest transitions are due to the $|1J''\rangle \to |0J\rangle$ components. This also means that, taking the experimental transition probabilities as benchmarks, we may improve our theoretical values by improving the quality of our eigenvectors.

TABLE I. Comparison of theoretical and experimental energies of selected excited odd-parity levels $|\beta''J''\rangle$ of erbium, of transition probabilities characterizing the spontaneous emission from levels $|\beta''J''\rangle$ to the ground level $|0J\rangle = |4f^{12}6s^2\,{}^3H_6\rangle$, and of the weight of the component $|1J''\rangle = |4f^{12}({}^3H_6).6s6p({}^1P_1^o)(6,1)^o_{J''}\rangle$ in the eigenvector associated with level $|\beta''J''\rangle$ [see Eq. (32)]. Theoretical quantities, in the columns "Theor.," come from our previous work [45], whereas experimental ones, in the columns "Expt.," come from Ref. [57]. Experimental weights $w^{(J'')}_{\beta'',1}$ are given by Eq. (41). The selected excited levels are such that the experimental transition probability towards the ground level is higher than $10^7\ \mathrm{s}^{-1}$. Values in parentheses (n) indicate $\times 10^n$.

$E_{\beta''J''}$ (cm^{-1})			$A_{\beta''J'',0J}$ (s^{-1})		$w^{(J'')}_{\beta'',1}$ (%)	
Expt.	Theor.	J''	Expt.	Theor.	Expt.	Theor.
24083	24056	5	1.02(8)	9.34(7)	48	46
24457	24492	6	3.26(7)	2.16(7)	16	11
24943	24946	7	1.85(8)	2.08(8)	76	79
25159	25168	7	4.03(7)	1.27(7)	16	5
25163	25171	5	3.76(7)	4.60(7)	15	16
25393	25419	6	3.19(7)	1.86(7)	14	7
25598	25570	7	1.51(7)	5.50(6)	6	2
25682	25598	5	6.3(7)	4.28(7)	24	13
25880	26071	6	1.22(8)	9.68(7)	49	31
26237	26178	6	2.90(7)	8.43(7)	11	26

To illustrate the validity of our weight calculations, in Table II, we list the real part of the scalar contribution, as well as the imaginary part of the scalar, vector, and tensor contributions of the dynamic dipole polarizability at the frequency corresponding to a 1064-nm wavelength, for erbium, holmium, and dysprosium. The calculations are carried out using three methods. (i) The transition energies and squares of the transition dipole moments are taken from our full numerical modeling of the atomic spectra. In particular, the squares of the transition dipole moments are extracted from the Einstein coefficients, by reversing Eq. (27):

$$|\langle\beta''J''\|\mathbf{d}\|0J\rangle|^2 = \frac{3\pi\epsilon_0\hbar^4c^3(2J''+1)A_{\beta''J'',0J}}{(E_{\beta''J''}-E_{0J})^3}. \tag{42}$$

This corresponds to the columns entitled "Theor." in Table II. (ii) The transition energies and the squares of the transition dipole moments come from experimental measurements of the transition probabilities using Eq. (42); this corresponds to the columns entitled "Expt." in Table II. (iii) Polarizabilities are calculated using Eqs. (20) and (21); to that end, the weights $w^{(J'')}_{\beta'',1}$ are calculated by applying Eq. (41) with experimental data, and the quantities r_{6s6p} come from our fitting procedure of Einstein coefficients, namely, $r_{6s6p} = 3.551$ a.u. for Er [45], 3.648 a.u. for Dy [46], and 3.630 a.u. for Ho (see Sec. III; for dipole moments, 1 a.u. $= ea_0$, with a_0 the Bohr radius). This

TABLE II. Dynamic dipole polarizabilities of dysprosium, holmium, and erbium in their ground level, at the commonly used 1064-nm trapping wavelength. Namely, we give the real part of the scalar contribution (in atomic units; 1 a.u. $= e^2a_0^3/4\pi\epsilon_0$), as well as the imaginary part of the scalar, vector, and tensor contributions (in 10^{-7} a.u.). The last two lines list the vector-to-scalar and tensor-to-scalar ratios of the imaginary part. The columns "Theor." and "Expt." list the theoretical (see Refs. [45] and [46] and Sec. III C here) and experimental [55–57] transition energies and transition probabilities respectively. The columns "Eq. (41)" correspond to the application of Eqs. (20), (21), and (41).

		Dy ($^5I_8$)			Ho ($^4I^o_{15/2}$)			Er ($^3H_6$)		
Part	Contribution	Theor.	Expt.	Eq. (41)	Theor.	Expt.	Eq. (41)	Theor.	Expt.	Eq. (41)
Real	Scalar	193	177	188	187	160	186	164	155	170
Imaginary	Scalar	49.1	40.3	48.8	39.6	34.7	46.6	23.4	22.0	27.1
	Vector	11.3	12.9	15.2	19.1	17.0	17.1	17.4	11.2	12.4
	Tensor	5.8	−9.0	−11.3	4.9	5.5	9.2	−6.9	−5.4	−5.0
Vector/ scalar ratio		0.230	0.320	0.311	0.482	0.490	0.367	0.744	0.509	0.458
Tensor/ scalar ratio		0.118	−0.223	−0.244	0.124	0.159	0.197	−0.295	−0.245	−0.185

corresponds to the columns entitled "Eq. (41)" in Table II. The real parts of the vector and tensor contributions are pointless here, as they vanish with method (iii).

First, we see that the real part of the scalar polarizability is smaller with the Expt. method. This is particularly striking in the case of holmium. In comparison with the Theor. method, this is due to the smaller number of experimental transitions than of theoretical ones. In contrast, the number of transitions in the Expt. and Eq. (41) methods is the same; however, we saw in Table I that the experimental weights are overestimated. Indeed there are certainly transitions with upper levels having a small $|1J''\rangle$ character which have not been detected. This results in the underestimation of the denominator of Eq. (41) and, so, the overestimation of $w^{(J'')}_{\beta'',1}$. Similar discrepancies are visible for the imaginary part of the scalar polarizability. Therefore it is appropriate to analyze the vector-to-scalar and tensor-to-scalar ratio contributions, in order to determine the anisotropy of the photon-scattering rate. The overall agreement of those ratios is good, and the two following trends are visible with the three methods: (i) In absolute value, the vector-to-scalar ratios are higher than the tensor-to-scalar ones; and (ii) the ratios are higher for erbium than for holmium, and *a fortiori* for dysprosium. Beyond these general features, it is worthwhile to examine each atom separately.

Erbium is the atom for which the anisotropy is the most pronounced, for both the vector and the tensor contributions, even if the ratios vary significantly from one method to the other. From the Eq. (41) method to the Theor. method, the ratios $\mathrm{Im}(\alpha_{\mathrm{vect}})/\mathrm{Im}(\alpha_{\mathrm{scal}})$ and $\mathrm{Im}(\alpha_{\mathrm{tens}})/\mathrm{Im}(\alpha_{\mathrm{scal}})$ range from 0.458 and −0.185 to 0.744 and −0.295, respectively.

In the case of dysprosium, the agreement between the Expt. and the Eq. (41) methods is very good. The ratios $\mathrm{Im}(\alpha_{\mathrm{vect}})/\mathrm{Im}(\alpha_{\mathrm{scal}})$ are equal to 0.320 and 0.311, and the ratios $\mathrm{Im}(\alpha_{\mathrm{tens}})/\mathrm{Im}(\alpha_{\mathrm{scal}})$ to −0.223 and −0.244, respectively. With the Theor. method, the ratios are lower, ($\mathrm{Im}(\alpha_{\mathrm{vect}})/\mathrm{Im}(\alpha_{\mathrm{scal}}) = 0.230$ and $\mathrm{Im}(\alpha_{\mathrm{tens}})/\mathrm{Im}(\alpha_{\mathrm{scal}}) = 0.118$), especially because this method does not allow for describing the CI mixing in the levels at 23 832 and 23878 cm^{-1}, and so it underestimates Eq. (38).

Finally, the case of holmium is hard to analyze, since no particular trend comes out of the calculations. The real part of the scalar polarizability is 27 a.u. smaller in the Expt. method than in the two others. Moreover, regarding the experimental transitions towards the ground level, none of them imply an upper level with an energy above 25 571 cm^{-1}. These two facts suggest the possibility that some strong transitions have not been detected, especially with upper levels $J'' = 13/2$. For instance, in our full numerical modeling of the Ho spectrum (see Sec. III B) we predict two such transitions, with unobserved upper levels: one with $E^{\mathrm{th}}_{\beta'',13/2} = 28\,014\,\mathrm{cm}^{-1}$, $w^{(13/2)}_{\beta'',1} = 4\%$, $A^{\mathrm{th}}_{\beta'',13/2,0J} = 2.61 \times 10^7\,\mathrm{s}^{-1}$ and the other with $E^{\mathrm{th}}_{\beta'',13/2} = 30\,942\,\mathrm{cm}^{-1}$, $w^{(13/2)}_{\beta'',1} = 7\%$, $A^{\mathrm{th}}_{\beta'',13/2,0J} = 1.89 \times 10^7\,\mathrm{s}^{-1}$.

III. MODELING OF THE HOLMIUM SPECTRUM

In order to calculate the different components of the polarizabilities, and also the various C_6 coefficients, using the sum-over-state formulas, one needs an extensive set of transition energies and transition dipole moments. This section is devoted to the full numerical calculations of those quantities, in the case of holmium in its ground $^4I^o_{15/2}$ and first excited level $^4I^o_{13/2}$. Indeed the transition between those two levels, allowed in the electric-quadrupole and magnetic-dipole approximations, was suggested as a candidate for optical clocks [19,21], as these levels are expected to possess very similar polarizabilities.

As the principle of our calculations [47–49] is identical to that in our previous work on dysprosium [46], we only highlight in this section the particularities of holmium. One of them is the rarity of experimental Landé g factors, which gives to our work a predictive character in this respect. The experimental energies are published in the NIST database [54], constructed from the critical compilation of Martin *et al.* [59] and from Ref. [60], which is more recent than the compilation. For odd-parity levels, we also use unpublished work from our group [61]. Note that ^{165}Ho, which is bosonic, possesses a nuclear spin $I = 7/2$, but the resulting hyperfine structure is not considered in the present article.

A. Energy levels

The ground level of holmium is of odd parity, with the configuration $4f^{11}6s^2$ and total electronic angular momentum $J = 15/2$. Table III presents a comparison of our

TABLE III. Comparison of energies E through the quantity $\Delta E = E^{\rm expt} - E^{\rm th}$ and Landé g factors g_L of Ho I odd-parity levels of the lowest electronic configuration [Xe]$4f^{11}6s^2$. The superscript "expt" indicates experimental values, which are taken from [54] and [60]. The superscript "th" indicates theoretical values from the parametric study in Ref. [61].

Term	J	$E^{\rm expt}$ (cm^{-1})	ΔE (cm^{-1})	$g_L^{\rm expt}$	$g_L^{\rm th}$	% leading term
^{4}I^o	15/2	0	30	1.195	1.197	97
$^4I^o$	13/2	5419.70	7	–	1.107	99
$^4I^o$	11/2	8605.16	−6	1.012	0.985	85
$^4I^o$	9/2	10695.75	−5	0.866	0.864	60
$^4F^o$	9/2	13094.42	46	–	1.174	65
$^4G^o$	11/2	22593.53	−90	–	1.193	44

theoretical energies and Landé g factors versus their experimental counterparts. The theoretical values are obtained in a calculation including the configurations $4f^{11}6s^2$, $4f^{11}5d6s$, and $4f^{10}6s^26p$ [61]. The levels of the $4f^{11}6s^2$ configuration can be labeled in the LS coupling scheme; for example, the orbital $L = 6$ and spin $S = 3/2$ angular momenta of the ground level are good quantum numbers up to 97%. By contrast, the level at 22 593.53 cm^{-1} is of ^4G and ^2H characters up to 44% and 36%, respectively

In the even parity, the electronic configurations included in our model are the two lowest ones, $4f^{11}6s6p$ and $4f^{10}5d6s^2$ [62], which are connected to the ground-state configuration $4f^{11}6s^2$ by electric-dipole transitions. Therefore, in our model, we neglect the configuration interaction with other even-parity configurations, especially $4f^{10}5d^26s$, which contains a large number of levels. By contrast, the first parametric study of even-parity levels was performed with configurations with a limited number of LS terms of the $4f^{10}$ and $4f^{11}$ cores, including a configuration interaction with $4f^{10}5d^26s$; but such a truncation strongly damaged the quality of the Hamiltonian eigenvectors [63]. In the present study, 92 even-parity levels were fitted to their known experimental counterparts [54,60], using 21 free energetic parameters, giving a 45-cm^{-1} standard deviation.

A comparison between theoretical and experimental levels is reported in Table VIII, while the fitted parameters are listed in Table IX (see the Appendix). Due to the lack of experimental g-factor data for most levels, we just list the theoretical results. All energies are given relative to the experimental $4f^{11}6s^2\,{}^4I^o_{15/2}$ ground level. Despite the absence of the $4f^{10}5d^26s$ configuration, whose lowest classified level is at 20 167.17 cm^{-1}, the agreement is very satisfactory.

B. Transition probabilities

Now that the energy parameters have been adjusted, the eigenvalues and eigenvectors of the Hamiltonian operator are fixed. The transition probabilities also depend on the MTDMs $-er_{n\ell,n''\ell''}$, whose adjustment using least-squares fitting between theoretical and experimental transition probabilities is the goal of this subsection.

Due to the configurations that we consider, two MTDMs come into play, r_{6s6p} and r_{4f5d}, corresponding, respectively, to the couples of configurations $4f^{11}6s^2$-$4f^{11}6s6p$ and $4f^{11}6s^2$-$4f^{10}5d6s^2$. The least-squares fitting procedure between theoretical and experimental Einstein coefficients is performed on the scaling factors (SFs) $f_1 = r_{6s6p}/r^{\rm HFR}_{6s6p}$ and $f_2 = r_{4f5d}/r^{\rm HFR}_{4f5d}$, rather than the MTDMs themselves. This allows for more direct comparisons with the results for dysprosium and erbium. Note that $r^{\rm HFR}_{n\ell,n''\ell''}$ stands for the *ab initio* values calculated with the Hartree-Fock method including relativistic corrections (HFR).

As references, we take the measured transition probabilities in Ref. [56]. We retain the transitions involving the ground and first excited levels and upper levels with energies lower than 30 000 cm^{-1}. Indeed the levels above 30 000 cm^{-1} are hard to classify unambiguously in configurations $4f^{10}5d6s^2$ and $4f^{11}6s6p$. In addition, in the list in Ref. [56], we can see some strong transitions whose upper level does not belong to the $4f^{11}6s6p$ or $4f^{10}5d6s^2$ configuration (according to the NIST database [54]), e.g., $E^{\rm expt}_{\beta''J''} = 24\,263.88$ cm^{-1}, $J'' = 17/2$, but is very close in energy to a $4f^{11}6s6p$ level with the same J'', e.g., $E^{\rm expt}_{\beta''J''} = 24\,360.81$ cm^{-1}. In contrast there is only one close theoretical level predicted, $E^{\rm th}_{\beta''J''} = 24\,354.1$ cm^{-1}. Similarly to the case for dysprosium, we can assume that the eigenvector of that theoretical level contains some components of the $|1J''\rangle$ state which is shared by the two "real" levels. In these particular cases, we compare our theoretical Einstein coefficient with the sum of the experimental ones. In Table IV, the two transitions labeled "mixed" correspond to that situation.

Due to strong differences between experimental and theoretical Einstein coefficients, we excluded six transitions (one with a high ratio, $A^{\rm th}_{\beta''J'',\beta J}/A^{\rm exp}_{\beta''J'',\beta J}$, and another four with

TABLE IV. Transitions excluded from the least-squares fitting procedure. The labels $|\beta''J''\rangle$ and $|\beta J\rangle$ correspond to upper and lower levels, respectively. The superscript "expt" indicates experimental values, which are taken from [56]. The transition wave number $\sigma_{\beta''J'',\beta J} = (E_{\beta''J''} - E_\beta)/2\pi\hbar c$ is in the vacuum. Values in parentheses (n) indicate $\times 10^n$. A blank in the column "removal reason" indicates that the upper level belongs neither to the $4f^{10}6s6p$ nor to the $4f^95d6s^2$ configuration. r., ratio.

$E^{\rm expt}_{\beta''J''}$ (cm^{-1})	J''	$E^{\rm expt}_{\beta J}$ (cm^{-1})	J	$\sigma^{\rm expt}_{\beta''J'',\beta J}$ (cm^{-1})	$A^{\rm expt}_{\beta''J'',\beta J}$ (s^{-1})	Removal reason
20258	6.5	0	7.5	20258	3.40(5)	
24014	6.5	0	7.5	24014	1.06(8)	Large r.
24264	8.5	0	7.5	24264	1.42(7)	Mixed[a]
24377	7.5	0	7.5	24377	5.78(6)	Mixed[b]
24760	6.5	0	7.5	24760	1.20(6)	
17059	6.5	5420	6.5	11640	0.34(3)	Large r.
18756	7.5	5420	6.5	13337	1.92(4)	Small r.
18858	6.5	5420	6.5	13438	0.91(4)	Small r.
20258	6.5	5420	6.5	14839	0.42(5)	
24760	6.5	5420	6.5	19340	0.47(4)	
25571	6.5	5420	6.5	20151	0.38(5)	Small r.
20241	6.5	8605	5.5	11636	1.19(4)	Small r.
20258	6.5	8605	5.5	11653	0.20(4)	
22978	6.5	8605	5.5	14373	4.28(4)	Small r.
24760	6.5	8605	5.5	16155	0.48(4)	

[a]Mixed with level at 24 361 cm^{-1}.
[b]Mixed with level at 24 661 cm^{-1}.

TABLE V. Comparison of Einstein A coefficients. The superscript "expt" indicates experimental values, which are taken from [56]. The superscript "th" indicates theoretical values from the present calculations. Values in parentheses (n) indicate $\times 10^n$. Values followed by an asterisk correspond to sums of experimental Einstein coefficients (see Table IV).

$E^{\rm expt}_{\beta'' J''}$ (cm^{-1})	J''	$E^{\rm expt}_{\beta J}$ (cm^{-1})	J	$\sigma^{\rm expt}_{\beta'' J'',\beta J}$ (cm^{-1})	$A^{\rm expt}_{\beta'' J'',\beta J}$ (s^{-1})	$A^{\rm th}_{\beta'' J'',\beta J}$ (s^{-1})
16710	8.5	0	7.5	16710	9.20(5)	1.51(6)
16882	7.5	0	7.5	16882	3.60(5)	7.91(5)
17059	6.5	0	7.5	17059	6.50(5)	1.25(6)
18652	7.5	0	7.5	18652	2.99(5)	2.19(5)
18756	7.5	0	7.5	18756	2.20(5)	5.77(4)
18858	6.5	0	7.5	18858	2.70(5)	2.87(5)
20075	7.5	0	7.5	20075	1.11(6)	6.24(5)
20241	6.5	0	7.5	20241	2.15(6)	1.72(6)
22978	6.5	0	7.5	22978	9.30(6)	1.18(7)
23445	7.5	0	7.5	23445	3.70(6)	3.62(6)
23499	8.5	0	7.5	23499	1.00(7)	1.13(7)
23835	7.5	0	7.5	23835	3.88(6)	2.79(6)
23956	6.5	0	7.5	23956	3.12(7)	2.23(7)
24361	8.5	0	7.5	24361	2.18(8)*	2.18(8)
24661	7.5	0	7.5	24661	2.06(8)*	2.14(8)
24741	6.5	0	7.5	24741	4.48(7)	3.08(7)
25273	7.5	0	7.5	25273	6.30(6)	8.32(6)
25571	6.5	0	7.5	25571	5.24(5)	5.08(5)
16882	7.5	5420	6.5	11463	6.00(3)	4.92(3)
20075	7.5	5420	6.5	14655	5.40(4)	7.48(3)
20241	6.5	5420	6.5	14822	2.58(5)	3.38(4)
22413	5.5	5420	6.5	16993	8.70(5)	1.51(6)
22978	6.5	5420	6.5	17558	2.60(5)	3.94(4)
24741	6.5	5420	6.5	19321	3.52(5)	8.96(4)
25273	7.5	5420	6.5	19853	2.99(4)	1.82(4)
29070	5.5	5420	6.5	23650	1.06(8)	1.11(8)
29097	5.5	5420	6.5	23677	6.70(6)	2.80(6)
29643	7.5	5420	6.5	24223	2.12(8)	2.13(8)
29752	6.5	5420	6.5	24332	2.00(8)	1.92(8)
25571	6.5	8605	5.5	16966	7.50(5)	1.39(6)

very low ratios). Special attention should be paid to the strong transition between the ground level and the excited $J'' = 13/2$ level at $E^{\rm expt}_{\beta'' J''} = 24\,014.2\,{\rm cm}^{-1}$. For the optimal scaling factors f_1 and f_2 (see below), the error in the other strongest transitions (above 10^8 s^{-1}) is below 5%, while for the latter it is 14%. This may be due to an underestimated experimental value. Another possible explanation is the following: There is a close $J'' = 6.5$ level, at $E^{\rm expt}_{\beta'' J''} = 23\,955.69\,{\rm cm}^{-1}$, where comparing the sum of transition probabilities implying these two upper levels, the theory-experiment agreement is very good (1.47 and 1.42×10^8 s^{-1}, respectively). The agreement for individual transitions can probably be improved by better CI mixing between the configurations $4f^{11}6s6p$ and $4f^{10}5d6s^2$.

We fitted the SFs using the remaining 29 transitions and found optimal SFs $f_1 = 0.798$ and $f_2 = 0.969$, corresponding to a standard deviation in Einstein coefficients [see Ref. [45], Eq. (15)] $\sigma_A = 4.14 \times 10^6$ s^{-1}. In particular the five strongest transitions are calculated with a precision better than 5%. Then, because the experimental Einstein coefficients in Ref. [56] are given with uncertainties reaching up to 10%, we made 10 000 fits in which all the experimental A coefficients have a random value within their uncertainty range. We obtain optimal SFs with statistical uncertainties: $f_1 = 0.799 \pm 0.010$ and $f_2 = 0.97 \pm 0.24$. The standard deviation is therefore much more sensitive to r_{6s6p} than to r_{4f5d}, since it involves the strongest transitions [45,46,48]. In what follows, we take the optimal scaling factors $f_1 = 0.799$ and $f_2 = 0.97$, for which a comparison between experimental and theoretical transition probabilities involving the two lowest levels of Ho I is presented in Table V. Using these optimal SFs, we can also calculate transition probabilities, which have not been measured and which are available upon request to the authors. In particular, as discussed in Sec. II D, we predict two strong transitions with unobserved upper levels of $J'' = 13/2$.

C. Dynamic dipole polarizability

The optimal set of spectroscopic data obtained in the previous subsection is now used to compute the real and imaginary parts of the scalar, vector, and tensor polarizabilities given by Eqs. (7)–(12). The squared transition dipole moments appearing in the sum are extracted from theoretical Einstein coefficients using Eq. (42).

To compare our results with the literature, the scalar, vector, and tensor static dipole polarizabilities are listed in Table VI, as well as the dynamic ones for the widespread laser-trapping

TABLE VI. Real and imaginary parts of the scalar, vector, and tensor dynamic dipole polarizabilities, at wave numbers $\sigma = \omega/2\pi c = 0$ and 9398 cm^{-1} (corresponding to $\lambda = 1064$ nm), for the ground $^4I^o_{15/2}$ and first excited $^4I^o_{13/2}$ levels of holmium. Our results are compared with available literature values.

	σ	Real part (a.u.)			Imaginary part (10^{-7} a.u.)		
Level	(cm^{-1})	Scalar	Vector	Tensor	Scalar	Vector	Tensor
$^4I^o_{15/2}$	0	160	0	−2.3	25.1	0	3.4
		159 [65], 170 [66]		−3.19 [66]			
		156 [67], 161 [68]		−1.17 [69]			
	9398	187	1.1	−3.5	39.6	19.1	4.9
$^4I^o_{13/2}$	0	160	0	−2.0	24.1	0	1.4
	9398	187	1.0	−3.0	38.3	17.7	2.0

wavelength $\lambda = 1064$ nm (corresponding to a wave number $\sigma = 9398\,\text{cm}^{-1}$). As one can note for the ground-level scalar polarizability, the agreement is good between the different theoretical results and with the new experimental one (for which we do not have any numerical value [64]). The tensor static polarizability is much smaller than the scalar one in all sources. For the $^4I^o_{13/2}$ level there are no literature values to our knowledge. They are actually very similar to those of the ground level, which supports the possibility of using these levels in a clock transition.

For both levels, the main result obtained in our previous work on erbium [45] and dysprosium [46] is confirmed. Regarding the real part, the vector and tensor polarizabilities are much smaller than the scalar one. The trapping potential is thus mostly isotropic, as it hardly depends on the electric-field polarization or the atomic azimuthal quantum number. By contrast, the tensor, especially the vector contributions of the imaginary part, represent a significant fraction of the scalar contribution, which makes photon scattering anisotropic. In Sec. II D, this anisotropy is discussed in detail and compared with the results on neighboring atoms.

These features are confirmed in Figs. 1 and 2, which present the real and imaginary, respectively, parts of the scalar, vector, and tensor polarizabilities as functions of the field wavelength λ and wave number $\sigma = 1/\lambda = \omega/2\pi c$ (c being the speed of light). We present our results in atomic units and the corresponding relevant quantities in physical units. The real part of the polarizability is associated with the potential energy $\overline{U}$, in equivalent temperatures of microkelvins (μK), obtained for a laser intensity of 1 GW/m^2. The imaginary part is associated with the photon-scattering rate $\overline{\Gamma}$, in inverse seconds (s^{-1}), for the same intensity. In Fig. 1(a), we also compare the real part of the scalar DDP given by our full numerical results and by the simplified model of Eq. (35) with $\omega_{6p} = 24\,320\,\text{cm}^{-1}$ and $r_{6s6p} = 3.630$ a.u. We see that the latter reproduces very nicely the background polarizability for both levels, but not the narrow peaks due to transition toward the levels of the $4f^{10}5d6s^2$ configuration or the intercombination lines toward the levels $4f^{11}(^4I^o_{15/2})6s6p(^3P^o_1)(15/2,1)_{J''}$ around 17 000 cm^{-1}.

D. van der Waals C_6 coefficients

Using the optimal spectroscopic data in Sec. III B, we can also compute the van der Waals C_6 coefficients, which also consist of a sum on the transition energies and transition dipole moments [70,71]. The van der Waals interaction between two open-shell atoms actually depends on a limited number of coefficients C_{6,k_Ak_B}, where the indices k_A and k_B correspond to the rank of irreducible tensors [46,72]. Giving diagonal matrix elements, the coefficient $C_{6,00}$ is referred to as isotropic, while the other C_{6,k_Ak_B} are called anisotropic. Table VII lists our calculated C_{6,k_Ak_B} coefficients for the two lowest levels of holmium. For any pair of levels, and similarly to the case of erbium [45] and dysprosium [46], the isotropic coefficient $C_{6,00}$ strongly dominates the anisotropic ones. Moreover, the coefficients are very similar for the three pairs of levels, because the polarizabilities of levels $^4I^o_{15/2}$ and $^4I^o_{13/2}$ are almost equal (see Table VI).

IV. CONCLUSION

In this article, we have derived a simplified model to characterize the optical trapping of ultracold lanthanide atoms. We have calculated analytically the real and imaginary parts of the scalar, vector, and tensor polarizabilities, assuming that the transitions involving valence electrons are the only ones present in the sum-over-state formula. We have given an analytical expression for the contribution from all the levels belonging to a given electronic configuration; this expression depends on only two parameters—an effective transition energy and an effective transition dipole moment. When applied to the two lowest levels of holmium, our model nicely reproduces the calculations based on the detailed modeling of the even-parity levels of holmium. We expect our simplified model to properly estimate the polarizabilities of levels of the $4f^q6s6p$ configuration, which are relevant for trapping but which

TABLE VII. C_6 coefficients (in atomic units), characterizing the van der Waals interactions between holmium atoms in the ground $^4I^o_{15/2}$ or first excited $^4I^o_{13/2}$ level, as functions of the pairs of indices k_A, k_B [46,72]. The case $k_A = k_B = 0$ corresponds to the so-called isotropic C_6 coefficient [70]. A 0 corresponds to an absolute value smaller than 0.1 a.u.

k_A, k_B	$^4I^o_{15/2}$-$^4I^o_{15/2}$	$^4I^o_{15/2}$-$^4I^o_{13/2}$	$^4I^o_{13/2}$-$^4I^o_{13/2}$
0, 0	−2214	−2214	−2214
1, 1	0	0	0
2, 0	−8.0	−8.0	−7.3
0, 2	−8.0	−7.3	−7.3
2, 2	0	0	0

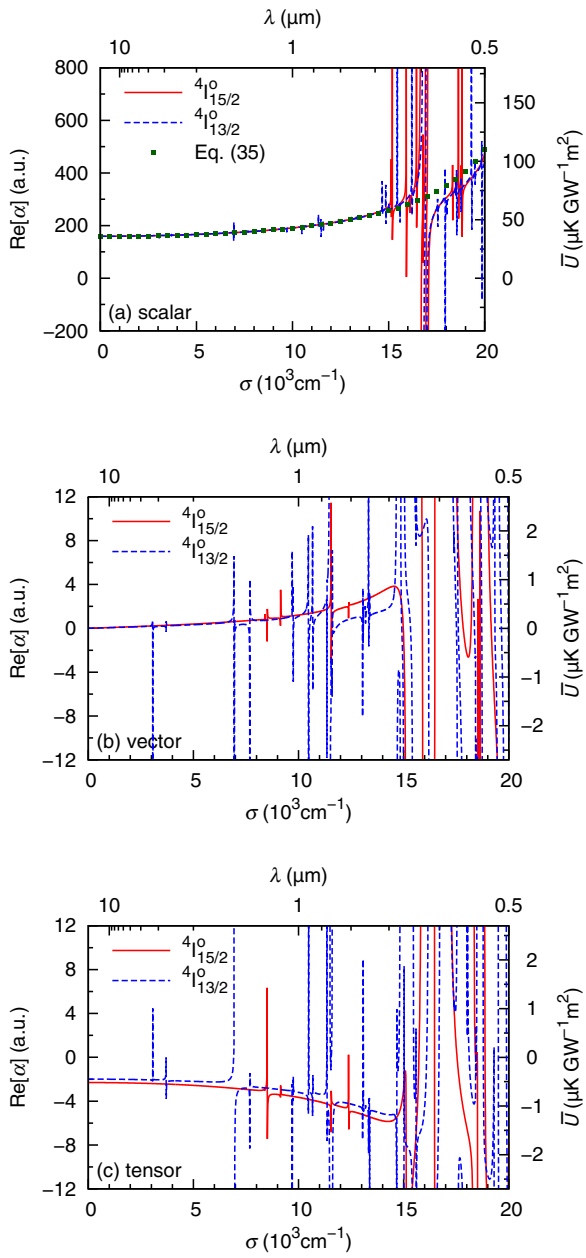

FIG. 1. Real part of the (a) scalar, (b) vector, and (c) tensor dynamic dipole polarizabilities of the $^4I^o_{15/2}$ and $^4I^o_{13/2}$ levels (in atomic units) and corresponding trap depths obtained for an intensity of 1 GW · m^{-2}, as functions of the trapping wave number σ and wavelength λ. In (a) the real part of the scalar polarizability given by Eq. (35) is also displayed.

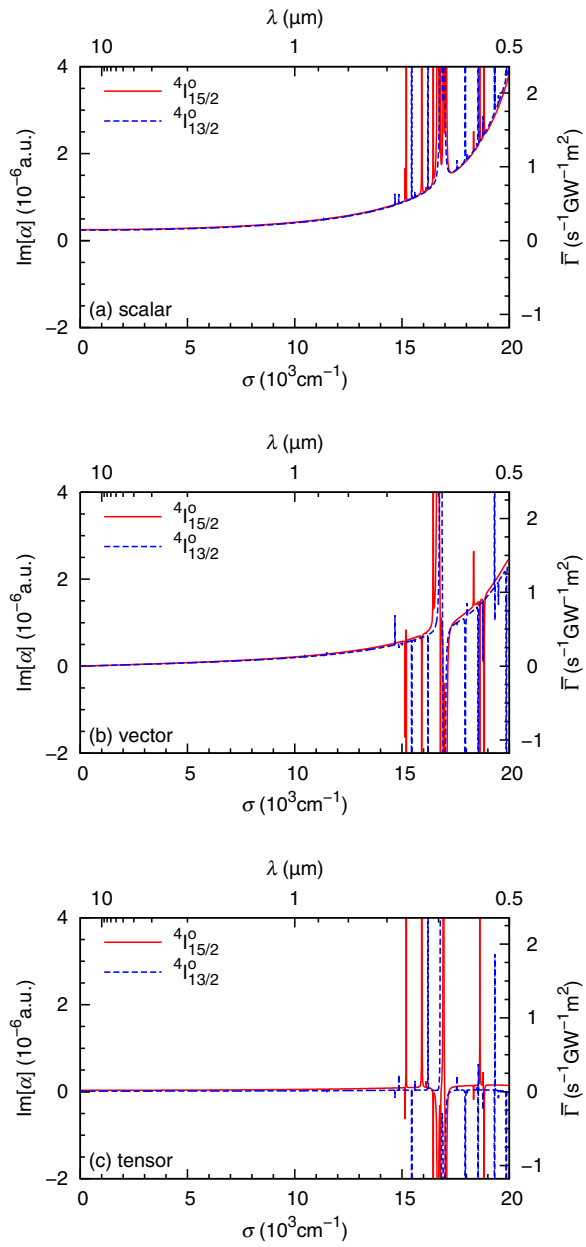

FIG. 2. Imaginary part of the (a) scalar, (b) vector, and (c) tensor dynamic dipole polarizabilities of the $^4I^o_{15/2}$ and $^4I^o_{15/2}$ levels (in atomic units) and corresponding photon-scattering rates obtained for an intensity of 1 GW · m^{-2}, as functions of the trapping wave number σ and wavelength λ.

involve highly excited levels, for example, of configurations $4f^q6s6d$ and $4f^q6p^2$, rarely known experimentally. In this respect, the future study of thulium will be particularly interesting, since high-lying excited states have been characterized in detail, and so the simplified expressions given in the present paper will be compared with those involving individual transition energies and transition dipole moments.

Regarding the ground level of lanthanides, we have also studied the influence of configuration interaction between $4f^q6s6p$ and other configurations. We have demonstrated that the real part of the polarizability is insensitive to configuration interaction and that the vector and tensor polarizabilities are vanishingly small. By contrast, the imaginary part turns out to be very sensitive to configuration interaction among excited levels; the latter is responsible for a decrease in the scalar contribution and for an increase in the vector and tensor ones. By comparing our numerical results for dysprosium, holmium, and erbium, we have found significant variations of the imaginary part of the various polarizabilities. For example, the scalar contribution for erbium is roughly twice as small as that for dysprosium, which tends to prove that

TABLE VIII. Same as Table III, for Ho I even-parity levels. Theoretical energies $E^{\rm th}$, Landé factors $g_L^{\rm th}$, leading configurations, leading LS terms, and their percentages in the eigenvectors, are derived by means of the Cowan code RCG with the parameter set reported in Table IX. In the configuration notations, A stands for $4f^{11}$, B for $4f^{10}$, ds^2 for $5d6s^2$, and sp for $6s6p$. Lowercase letters or Arabic numbers in the seventh column correspond to different possible parent terms [49]. Terms in parentheses are associated with the core configuration A or B.

$E^{\rm expt}$ (cm^{-1})	$E^{\rm th}$ (cm^{-1})	ΔE (cm^{-1})	$g_L^{\rm th}$	Leading configuration	%	Leading LS term
			$J = 7/2$			
32758.37	32750.2	8	1.253	$B - ds^2$	15	$B - ds^2(^5S)^4D$
32931.51	32935.7	−4	1.232	$B - ds^2$	25	$B - ds^2(^5F)^4G$
33188.42	33202.1	−14	0.926	$B - ds^2$	37	$B - ds^2\,(^5F)^4H$
35078.45	35105.5	−27	1.147	$B - ds^2$	19	$B - ds^2\,(^5G)^6D$
36001.87	35991.9	10	1.074	$B - ds^2$	13	$B - ds^2\,(^5G)^6G$
36504.15	36486.6	18	1.114	$B - ds^2$	9	$B - ds^2\,(^5G)^4F$
			$J = 9/2$			
16719.62	16727.3	−8	1.118	$B - ds^2$	40	$B - ds^2\,(^5I)^6G$
18757.87	18682.1	76	0.991	$B - ds^2$	47	$B - ds^2\,(^5I)^6I$
21373.01	21371.6	1	1.140	$B - ds^2$	62	$B - ds^2\,(^5I)^4G$
23861.17	23909.6	−48	0.980	$A - sp$	32	$A - sp\,(^4I)^6H$
24355.64	24367.3	−12	1.137	$B - ds^2$	27	$B - ds^2\,(^5I)^4H$
25453.49	25427.1	26	0.906	$A - sp$	30	$A - sp\,(^4I)^6I$
26039.99	25991.7	48	0.831	$B - ds^2$	48	$B - ds^2\,(^5I)^4I$
28638.41	28653.1	−15	1.456	$B - ds^2$	54	$B - ds^2\,(^5S)^6D$
32039.69	32053.7	−14	1.247	$B - ds^2$	20	$B - ds^2\,(^5G)^6D$
33577.20	33553.1	24	1.159	$B - ds^2$	18	$B - ds^2\,(^5F)^4G$
35270.88	35269.7	1	1.137	$B - ds^2$	11	$B - ds^2\,(^5G)^6D$
			$J = 11/2$			
13082.93	13094.9	−12	1.260	$B - ds^2$	50	$B - ds^2\,(^5I)^6G$
15792.13	15805.2	−13	1.143	$B - ds^2$	37	$B - ds^2\,(^5I)^6I$
16937.43	16958.5	−21	1.244	$B - ds^2$	52	$B - ds^2\,(^5I)^4G$
18491.21	18465.0	26	1.107	$B - ds^2$	25	$B - ds^2\,(^5I)^6H$
18821.25	18802.1	19	1.107	$A - sp$	46	$A - sp\,(^4I)^2H$
20493.40	20427.2	66	0.903	$B - ds^2$	56	$B - ds^2\,(^5I)^6K$
20849.13	20863.0	−14	1.104	$B - ds^2$	32	$B - ds^2\,(^5I)^4H$
22413.14	22378.1	35	1.078	$A - sp$	29	$A - sp\,(^4I)^6H$
23379.31	23361.4	18	1.065	$B - ds^2$	29	$B - ds^2\,(^5I)^4I$
23946.16	23961.3	−15	1.057	$A - sp$	30	$A - sp\,(^4I)^6H$
24141.21	24179.4	−38	1.276	$B - ds^2$	37	$B - ds^2\,(^5F)^6F$
24830.43	24907.2	−77	0.968	$A - sp$	27	$A - sp\,(^4I)^6K$
25261.55	25271.4	−10	0.864	$B - ds^2$	44	$B - ds^2\,(^5I)^4K$
25503.33	25467.7	36	0.998	$A - sp$	14	$A - sp\,(^4I)^6K$
25914.31	25997.5	−83	1.209	$B - ds^2$	32	$B - ds^2\,(^5F)^6H$
28793.03	28824.0	−31	1.230	$B - ds^2$	48	$B - ds^2\,(^5F)^4G$
29069.78	29016.7	53	1.154	$A - sp$	33	$A - sp\,(^4I)^4Hb$
29096.77	29132.9	−36	1.078	$A - sp$	19	$A - sp\,(^4F)^6F$
30423.60	30332.7	91	1.240	$B - ds^2$	39	$B - ds^2\,(^5F)^6G$
31903.28	31862.7	41	1.227	$B - ds^2$	18	$B - ds^2\,(^5F)^6G$
32837.21	32860.6	−23	1.014	$A - sp$	31	$A - sp\,(^4I)^4Ib$
33212.51	33287.1	−75	1.206	$A - sp$	23	$A - sp\,(^2H)^4G2$
33986.71	33965.6	21	1.104	$A - sp$	10	$A - sp\,(^2H)^2I2$
34270.67	34292.7	−22	1.141	$B - ds^2$	19	$B - ds^2\,(^5G)^4G$
			$J = 13/2$			
9147.08	9117.3	30	1.338	$B - ds^2$	66	$B - ds^2\,(^5I)^6G$
12344.55	12364.8	−20	1.236	$B - ds^2$	27	$B - ds^2\,(^5I)^6I$
15081.12	15112.6	−32	1.177	$B - ds^2$	46	$B - ds^2\,(^5I)^4H$
16735.95	16763.6	−28	1.200	$B - ds^2$	41	$B - ds^2\,(^5I)^6H$
17059.35	17019.9	39	1.193	$A - sp$	29	$A - sp\,(^4I)^4Ha$
18564.90	18493.2	72	1.050	$B - ds^2$	45	$B - ds^2\,(^5I)^6K$
18858.19	18792.4	66	1.138	$A - sp$	37	$A - sp\,(^4I)^2I$
20241.31	20266.4	−25	1.104	$B - ds^2$	43	$B - ds^2\,(^5I)^4I$

TABLE VIII. (*Continued.*)

E^{expt} (cm^{-1})	E^{th} (cm^{-1})	ΔE (cm^{-1})	g_L^{th}	Leading configuration	%	Leading LS term
21044.81	21012.1	33	0.887	$B-ds^2$	67	$B-ds^2\,(^5I)^6L$
21584.89	21623.2	−38	1.174	$A-sp$	27	$A-sp\,(^4I)^6H$
22157.86	22214.2	−56	1.059	$A-sp$	22	$A-sp\,(^4I)^4Ka$
22978.19	22969.7	08	1.013	$B-ds^2$	43	$B-ds^2\,(^5I)^4K$
24014.22	23908.9	105	1.199	$A-sp$	39	$A-sp\,(^4I)^4Hb$
23955.68	23968.7	−13	1.138	$A-sp$	32	$A-sp\,(^4I)^6I$
24740.52	24739.9	1	1.245	$B-ds^2$	36	$B-ds^2\,(^5F)^6H$
25571.15	25569.0	2	1.048	$A-sp$	34	$A-sp\,(^4I)^6K$
25930.66	25950.9	−20	0.831	$B-ds^2$	75	$B-ds^2\,(^5I)^4L$
27141.28	27143.8	−3	1.096	$A-sp$	23	$A-sp\,(^4I)^6I$
29751.91	29792.1	−40	1.098	$A-sp$	45	$A-sp\,(^4I)^4Ib$
33907.40	33780.7	127	1.196	$A-sp$	22	$A-sp\,(^2H)^4H2$
			$J=15/2$			
8427.11	8482.7	−56	1.279	$B-ds^2$	53	$B-ds^2\,(^5I)^6H$
12339.04	12352.2	−13	1.237	$B-ds^2$	36	$B-ds^2\,(^5I)^6H$
15136.06	15159.7	−24	1.170	$B-ds^2$	55	$B-ds^2\,(^5I)^4I$
15855.28	15892.2	−37	1.261	$A-sp$	55	$A-sp\,(^4I)^6H$
16154.21	16087.4	67	1.183	$B-ds^2$	28	$B-ds^2\,(^5I)^6I$
16882.28	16900.3	−18	1.125	$A-sp$	35	$A-sp\,(^4I)^2K$
18651.53	18600.1	51	1.196	$A-sp$	25	$A-sp\,(^4I)^4Ia$
18756.22	18744.3	12	1.029	$B-ds^2$	56	$B-ds^2\,(^5I)^6L$
20074.89	20083.9	−9	1.094	$B-ds^2$	35	$B-ds^2\,(^5I)^6K$
22227.34	22221.5	6	1.153	$A-sp$	42	$A-sp\,(^4I)^6K$
23445.28	23451.8	−6	1.010	$B-ds^2$	59	$B-ds^2\,(^5I)^4L$
23834.94	23842.2	−7	1.176	$A-sp$	43	$A-sp\,(^4I)^6I$
24660.80	24723.4	−63	1.189	$A-sp$	42	$A-sp\,(^4I)^4Ib$
25272.63	25270.0	3	1.299	$B-ds^2$	76	$B-ds^2\,(^5F)^6H$
26957.88	27015.9	−58	1.118	$A-sp$	25	$A-sp\,(^4I)^6K$
29642.95	29658.5	−16	1.093	$A-sp$	48	$A-sp\,(^4I)^4Kb$
37233.47	37253.2	−20	1.153	$B-ds^2$	16	$B-ds^2\,(^3L)^4I$
			$J=17/2$			
8378.91	8370.5	8	1.267	$B-ds^2$	73	$B-ds^2\,(^5I)^6I$
11530.56	11523.0	8	1.190	$B-ds^2$	52	$B-ds^2\,(^5I)^4K$
15130.31	15152.3	−22	1.148	$B-ds^2$	33	$B-ds^2\,(^5I)^6L$
16438.01	16421.3	17	1.147	$B-ds^2$	36	$B-ds^2\,(^5I)^6K$
16709.82	16640.0	70	1.229	$A-sp$	40	$A-sp\,(^4I)^6I$
18337.80	18305.2	33	1.239	$A-sp$	52	$A-sp\,(^4I)^6I$
20568.63	20589.1	−21	1.099	$B-ds^2$	47	$B-ds^2\,(^5I)^4L$
23498.57	23549.6	−51	1.197	$A-sp$	60	$A-sp\,(^4I)^6K$
24360.81	24354.1	7	1.176	$A-sp$	57	$A-sp\,(^4I)^4Ka$
			$J=19/2$			
9741.50	9772.5	−31	1.230	B–ds^2	67	B–$ds^2\,(^5I)^6K$
11689.77	11650.3	40	1.181	$B-ds^2$	57	$B-ds^2\,(^5I)^4L$
16683.52	16718.0	−34	1.176	$B-ds^2$	69	$B-ds^2\,(^5I)^6L$
17883.57	17897.5	−14	1.261	$A-sp$	97	$A-sp\,(^4I)^6K$
			$J=21/2$			
11322.31	11358.3	−36	1.232	$B-ds^2$	93	$B-ds^2\,(^5I)^6L$

configuration-interaction mixing is stronger in erbium. This is very surprising, as the density of levels of dysprosium is higher around 25 000 cm^{-1} and, so, *a priori* more favorable to configuration interaction. Again, the case of thulium will be particularly enlightening, because the large number of relatively strong transitions (with probabilities higher than 10^7 s^{-1}; see Ref. [58]) suggests even stronger configuration interaction than in erbium. Finally, we would like to emphasize that experimental measurements of heating rate or trap lifetimes are particularly welcome, in order to check the validity of our predictions.

ACKNOWLEDGMENTS

The authors acknowledge support from "DIM Nano-K" under the project "InterDy", and from Agence Nationale de la Recherche (ANR) under the project "COPOMOL" (Contract No. ANR-13-IS04-0004-01).

APPENDIX: EVEN-PARITY ENERGY LEVELS

This Appendix presents the detailed calculations of holmium even-parity levels. Table VIII reports the results of our calculations, including the discrepancy between theoretical and experimental energies. Table IX lists the optimal parameters after the least-squares fitting procedure on energies.

TABLE IX. Fitted parameters (in cm^{-1}) for even-parity configurations of Ho I compared with relativistic Hartree-Fock (HFR) values. The scaling factors are $SF(P) = P_{fit}/P_{HFR}$, except for E_{av}, where they equal $P_{fit} - P_{HFR}$. Some parameters are constrained to vary at a constant ratio r_n, indicated in the second column except when "fix" appears in the second or in the "Uncertainty" column. In this case, the parameter P is not adjusted. The Uncertainty columns list the standard error of each parameter after the fitting procedure.

Parameter	Constant	Fitted parameters				Fitted parameters			
P	ratio	P_{fit}	Uncertainty	P_{HFR}	SF	P_{fit}	Uncertainty	P_{HFR}	SF
E_{av}		59617	105	5940	53677	51079	64	15134	35945
$F^2(4f4f)$	r_1	94927	707	125792	0.755	89432	666	118509	0.755
$F^4(4f4f)$	r_2	66088	1446	78881	0.838	61977	1356	73975	0.838
$F^6(4f4f)$	r_3	48377	1350	56738	0.853	45289	1264	53115	0.853
α	r_4	23.0	4			23.0	4		
β	Fix	−650				−650			
γ	Fix	2000				2000			
ζ_{4f}	r_5	2141	4	2193	0.976	2009	4	2058	0.976
ζ_{5d}	r_7	757	11	920	0.823				
ζ_{6p}	r_{16}					1435	15	990	1.449
$F^1(4f5d)$	r_8	674	91						
$F^2(4f5d)$	r_9	15491	279	20639	0.751				
$F^4(4f5d)$	r_{10}	10954	464	9423	1.162				
$F^1(4f6p)$	Fix					150			
$F^2(4f6p)$	r_{17}					3643	289	3324	1.096
$G^1(4f5d)$	r_{11}	5410	151	8944	0.605				
$G^2(4f5d)$	r_{12}	1378	434						
$G^3(4f5d)$	r_{13}	6036	460	7086	0.852				
$G^4(4f5d)$	r_{14}	2314	546						
$G^5(4f5d)$	r_{15}	4508	306	5353	0.842				
$G^3(4f6s)$	r_{18}					1358	92	1676	0.810
$G^2(4f6p)$	Fix					760		760	1.0
$G^4(4f6p)$	Fix					662		662	1.0
$G^1(6s6p)$	r_{19}					10321	74	23282	0.443
Configuration interaction			$4f^{10}5d6s^2 - 4f^{11}6s6p$						
$R^1(5d6s,4f6p)$	r_6	−3223	150	−4555	0.708				
$R^3(5d6s,6p4f)$	r_6	−685	32	−968	0.708				

[1] A. Frisch, M. Mark, K. Aikawa, F. Ferlaino, J. L. Bohn, C. Makrides, A. Petrov, and S. Kotochigova, Quantum chaos in ultracold collisions of gas-phase erbium atoms, Nature **507**, 475 (2014).

[2] T. Maier, H. Kadau, M. Schmitt, M. Wenzel, I. Ferrier-Barbut, T. Pfau, A. Frisch, S. Baier, K. Aikawa, L. Chomaz, M. J. Mark, F. Ferlaino, C. Makrides, E. Tiesinga, A. Petrov, and S. Kotochigova, Emergence of Chaotic Scattering in Ultracold Er and Dy, Phys. Rev. X **5**, 041029 (2015).

[3] Y. Tang, A. Sykes, N. Q. Burdick, J. L. Bohn, and B. L. Lev, *s*-wave scattering lengths of the strongly dipolar bosons ^{162}Dy and ^{160}Dy, Phys. Rev. A **92**, 022703 (2015).

[4] M. Lu, N. Q. Burdick, and B. L. Lev, Quantum Degenerate Dipolar Fermi Gas, Phys. Rev. Lett. **108**, 215301 (2012).

[5] N. Nessi, A. Iucci, and M. A. Cazalilla, Quantum Quench and Prethermalization Dynamics in a Two-Dimensional Fermi Gas with Long-Range Interactions, Phys. Rev. Lett. **113**, 210402 (2014).

[6] A. Frisch, M. Mark, K. Aikawa, S. Baier, R. Grimm, A. Petrov, S. Kotochigova, G. Quéméner, M. Lepers, O. Dulieu, and F. Ferlaino, Ultracold Polar Molecules Composed of Strongly Magnetic Atoms, Phys. Rev. Lett. **115**, 203201 (2015).

[7] N. Y. Yao, S. D. Bennett, C. R. Laumann, B. L. Lev, and A. V. Gorshkov, Bilayer fractional quantum Hall states with dipoles, Phys. Rev. A **92**, 033609 (2015).

[8] S. Baier, M. J. Mark, D. Petter, K. Aikawa, L. Chomaz, Z. Cai, M. Baranov, P. Zoller, and F. Ferlaino, Extended Bose-Hubbard models with ultracold magnetic atoms, Science **352**, 201 (2016).

[9] T. Maier, I. Ferrier-Barbut, H. Kadau, M. Schmitt, M. Wenzel, C. Wink, T. Pfau, K. Jachymski, and P. S. Julienne, Broad universal Feshbach resonances in the chaotic spectrum of dysprosium atoms, Phys. Rev. A **92**, 060702 (2015).

[10] N. Q. Burdick, K. Baumann, Y. Tang, M. Lu, and B. L. Lev, Fermionic Suppression of Dipolar Relaxation, Phys. Rev. Lett. **114**, 023201 (2015).

[11] B. M. Fregoso, K. Sun, E. Fradkin, and B. L. Lev, Biaxial nematic phases in ultracold dipolar Fermi gases, New J. Phys. **11**, 103003 (2009).

[12] K. Aikawa, S. Baier, A. Frisch, M. Mark, C. Ravensbergen, and F. Ferlaino, Observation of Fermi surface deformation in a dipolar quantum gas, Science **345**, 1484 (2014).

[13] H. Kadau, M. Schmitt, M. Wenzel, C. Wink, T. Maier, I. Ferrier-Barbut, and T. Pfau, Observing the Rosensweig instability of a quantum ferrofluid, Nature **530**, 194 (2016).

[14] I. Ferrier-Barbut, H. Kadau, M. Schmitt, M. Wenzel, and T. Pfau, Observation of Quantum Droplets in a Strongly Dipolar Bose Gas, Phys. Rev. Lett. **116**, 215301 (2016).

[15] K.-T. Xi and H. Saito, Droplet formation in a Bose-Einstein condensate with strong dipole-dipole interaction, Phys. Rev. A **93**, 011604 (2016).

[16] A. Macia, J. Sánchez-Baena, J. Boronat, and F. Mazzanti, Droplets of Trapped Quantum Dipolar Bosons, Phys. Rev. Lett. **117**, 205301 (2016).

[17] X. Cui, B. Lian, T.-L. Ho, B. L. Lev, and H. Zhai, Synthetic gauge field with highly magnetic lanthanide atoms, Phys. Rev. A **88**, 011601 (2013).

[18] N. Q. Burdick, Y. Tang, and B. L. Lev, A Long-Lived Spin-Orbit-Coupled Degenerate Dipolar Fermi Gas, Phys. Rev. X **6**, 031022 (2016).

[19] A. Kozlov, V. A. Dzuba, and V. V. Flambaum, Prospects of building optical atomic clocks using Er I or Er III, Phys. Rev. A **88**, 032509 (2013).

[20] G. A. Vishnyakova, E. S. Kalganova, D. D. Sukachev, S. A. Fedorov, A. V. Sokolov, A. V. Akimov, N. N. Kolachevsky, and V. N. Sorokin, Two-stage laser cooling and optical trapping of thulium atoms, Laser Phys. **24**, 074018 (2014).

[21] D. Sukachev, S. Fedorov, I. Tolstikhina, E. Kalganova, G. Vishnyakova, K. Khabarova, D. Tregubov, A. Golovizin, V. Sorokin, and N. Kolachevsky, Inner-shell magnetic dipole transition in Tm atoms as a candidate for optical lattice clocks, Phys. Rev. A **94**, 022512 (2016).

[22] C. I. Hancox, S. C. Doret, M. T. Hummon, L. Luo, and J. M. Doyle, Magnetic trapping of rare-earth atoms at millikelvin temperatures, Nature **431**, 281 (2004).

[23] B. Hemmerling, G. K. Drayna, E. Chae, A. Ravi, and J. M. Doyle, Buffer gas loaded magneto-optical traps for Yb, Tm, Er and Ho, New J. Phys. **16**, 063070 (2014).

[24] N. Leefer, A. Cingöz, B. Gerber-Siff, A. Sharma, J. R. Torgerson, and D. Budker, Transverse laser cooling of a thermal atomic beam of dysprosium, Phys. Rev. A **81**, 043427 (2010).

[25] M. Lu, S. H. Youn, and B. L. Lev, Trapping Ultracold Dysprosium: A Highly Magnetic Gas for Dipolar Physics, Phys. Rev. Lett. **104**, 063001 (2010).

[26] T. Maier, H. Kadau, M. Schmitt, A. Griesmaier, and T. Pfau, Narrow-line magneto-optical trap for dysprosium atoms, Opt. Lett. **39**, 3138 (2014).

[27] D. Dreon, L. A. Sidorenkov, C. Bouazza, W. Maineult, J. Dalibard, and S. Nascimbene, Optical cooling and trapping of highly magnetic atoms: The benefits of a spontaneous spin polarization, J. Phys. B **50**, 065005 (2017).

[28] H. Ban, M. Jacka, J. Hanssen, J. Reader, and J. McClelland, Laser cooling transitions in atomic erbium, Opt. Express **13**, 3185 (2005).

[29] J. J. McClelland and J. L. Hanssen, Laser Cooling Without Repumping: A Magneto-Optical Trap for Erbium Atoms, Phys. Rev. Lett. **96**, 143005 (2006).

[30] A. Frisch, K. Aikawa, M. Mark, A. Rietzler, J. Schindler, E. Zupanič, R. Grimm, and F. Ferlaino, Narrow-line magneto-optical trap for erbium, Phys. Rev. A **85**, 051401 (2012).

[31] J. Miao, J. Hostetter, G. Stratis, and M. Saffman, Magneto-optical trapping of holmium atoms, Phys. Rev. A **89**, 041401 (2014).

[32] D. Sukachev, A. Sokolov, K. Chebakov, A. Akimov, S. Kanorsky, N. Kolachevsky, and V. Sorokin, Magneto-optical trap for thulium atoms, Phys. Rev. A **82**, 011405 (2010).

[33] M. Lu, N. Q. Burdick, S. H. Youn, and B. L. Lev, Strongly Dipolar Bose-Einstein Condensate of Dysprosium, Phys. Rev. Lett. **107**, 190401 (2011).

[34] Y. Tang, N. Q. Burdick, K. Baumann, and B. L. Lev, Bose-Einstein condensation of ^{162}Dy and ^{160} Dy, New J. Phys. **17**, 045006 (2015).

[35] K. Aikawa, A. Frisch, M. Mark, S. Baier, A. Rietzler, R. Grimm, and F. Ferlaino, Bose-Einstein Condensation of Erbium, Phys. Rev. Lett. **108**, 210401 (2012).

[36] K. Aikawa, A. Frisch, M. Mark, S. Baier, R. Grimm, and F. Ferlaino, Reaching Fermi Degeneracy via Universal Dipolar Scattering, Phys. Rev. Lett. **112**, 010404 (2014).

[37] M. Saffman and K. Mølmer, Scaling the neutral-atom Rydberg gate quantum computer by collective encoding in holmium atoms, Phys. Rev. A **78**, 012336 (2008).

[38] J. Hostetter, J. D. Pritchard, J. E. Lawler, and M. Saffman, Measurement of holmium Rydberg series through magneto-optical trap depletion spectroscopy, Phys. Rev. A **91**, 012507 (2015).

[39] B. K. Newman, N. Brahms, Y. S. Au, C. Johnson, C. B. Connolly, J. M. Doyle, D. Kleppner, and T. J. Greytak, Magnetic relaxation in dysprosium-dysprosium collisions, Phys. Rev. A **83**, 012713 (2011).

[40] W. Kao, Y. Tang, N. Q. Burdick, and B. L. Lev, Anisotropic dependence of tune-out wavelength near the Dy 741-nm transition, Optics Express **25**, 3411 (2017).

[41] T. Miyamachi, T. Schuh, T. Märkl, C. Bresch, T. Balashov, A. Stöhr, C. Karlewski, S. André, M. Marthaler, M. Hoffmann *et al.*, Stabilizing the magnetic moment of single holmium atoms by symmetry, Nature **503**, 242 (2013).

[42] M. Shiddiq, D. Komijani, Y. Duan, A. Gaita-Ariño, E. Coronado, and S. Hill, Enhancing coherence in molecular spin qubits via atomic clock transitions, Nature **531**, 348 (2016).

[43] N. L. Manakov, V. D. Ovsiannikov, and L. P. Rapoport, Atoms in a laser field, Phys. Rep. **141**, 320 (1986).

[44] R. Grimm, M. Weidemüller, and Y. B. Ovchinnikov, Optical dipole traps for neutral atoms, Adv. At. Mol. Opt. Phys. **42**, 95 (2000).

[45] M. Lepers, J.-F. Wyart, and O. Dulieu, Anisotropic optical trapping of ultracold erbium atoms, Phys. Rev. A **89**, 022505 (2014).

[46] H. Li, J.-F. Wyart, O. Dulieu, S. Nascimbène, and M. Lepers, Optical trapping of ultracold dysprosium atoms: Transition probabilities, dynamic dipole polarizabilities and van der Waals C_6 coefficients, J. Phys. B **50**, 014005 (2017).

[47] J.-F. Wyart, On the interpretation of complex atomic spectra by means of the parametric Racah–Slater method and Cowan codes, Can. J. Phys. **89**, 451 (2011).

[48] M. Lepers, Y. Hong, J.-F. Wyart, and O. Dulieu, Proposal for laser cooling of rare-earth ions, Phys. Rev. A **93**, 011401(R) (2016).

[49] R. D. Cowan, *The Theory of Atomic Structure and Spectra*, *Vol. 3* (University of California Press, Berkeley, 1981).

[50] K. Beloy, Theory of the ac stark effect on the atomic hyperfine structure and applications to microwave atomic clocks, Ph.D. thesis, University of Nevada, Reno, 2009.

[51] P. W. Langhoff, S. T. Epstein, and M. Karplus, Aspects of time-dependent perturbation theory, Rev. Mod. Phys. **44**, 602 (1972).

[52] D. A. Varshalovich, A. N. Moskalev, and V. K. Khersonskii, *Quantum Theory of Angular Momentum* (World Scientific, Singapore, 1988).

[53] J. R. P. Angel and P. G. H. Sandars, The hyperfine structure Stark effect. I. Theory, Proc. R. Soc. London A **305**, 125 (1968).

[54] A. Kramida, Yu. Ralchenko, J. Reader, and NIST ASD Team, *NIST Atomic Spectra Database (Version 5.3)* (National Institute of Standards and Technology, Gaithersburg, MD, 2015). Available at: http://physics.nist.gov/asd.

[55] M. E. Wickliffe, J. E. Lawler, and G. Nave, Atomic transition probabilities for Dy I and Dy II, J. Quant. Spectrosc. Radiat. Transfer **66**, 363 (2000).

[56] G. Nave, Atomic transition rates for neutral holmium (Ho I), J. Opt. Soc. Am. B **20**, 2193 (2003).

[57] J. E. Lawler, J. F. Wyart, and E. A. Den Hartog, Atomic transition probabilities of Er I, J. Phys. B **43**, 235001 (2010).

[58] M. E. Wickliffe and J. E. Lawler, Atomic transition probabilities for Tm I and Tm II, J. Opt. Soc. Am. B **14**, 737 (1997).

[59] W. C. Martin, R. Zalubas, and L. Hagan, Atomic energy levels—the rare-earth elements, Stand. Ref. Data Ser. (Natl. Bur. Stand., U.S.) **60**, 332 (1978).

[60] S. Kröger, J.-F. Wyart, and P. Luc, Theoretical interpretation of hyperfine structures in doubly-excited configurations $4f105d6s6p$ and $4f105d26s$ and new energy levels in neutral holmium (Ho I), Phys. Scripta **55**, 579 (1997).

[61] J.-F. Wyart, An interpretation of Dy I and Ho I energy levels in the ground state parity (unpublished).

[62] L. Brewer, in *Systematics of the Properties of the Lanthanides*, edited by S. P. Sinha and D. Reidel (Dordrecht, Netherlands, 1983).

[63] J.-F. Wyart, Interpretation du spectre de Dy I: I. Etude des configurations impaires, Physica **75**, 371 (1974).

[64] L. Ma, J. Indergaard, B. Zhang, I. Larkin, R. Moro, and W. A. de Heer, Measured atomic ground-state polarizabilities of 35 metallic elements, Phys. Rev. A **91**, 010501(R) (2015).

[65] D. R. Lide, *CRC Handbook of Chemistry and Physics* (CRC Press, Boca Raton, FL, 2012).

[66] X. Chu, A. Dalgarno, and G. C. Groenenboom, Dynamic polarizabilities of rare-earth-metal atoms and dispersion coefficients for their interaction with helium atoms, Phys. Rev. A **75**, 032723 (2007).

[67] V. A. Dzuba, A. Kozlov, and V. V. Flambaum, Scalar static polarizabilities of lanthanides and actinides, Phys. Rev. A **89**, 042507 (2014).

[68] V. A. Dzuba, Ionization potentials and polarizabilities of superheavy elements from Db to Cn ($z = 105$–112), Phys. Rev. A **93**, 032519 (2016).

[69] R.-H. Rinkleff and F. Thorn, On the tensor polarizabilities in the $4f^n6s^2$ ground levels of the neutral rare-earth atoms, Z. Phys. D **32**, 173 (1994).

[70] A. J. Stone, *The Theory of Intermolecular Forces* (Oxford University Press, New York, 1996).

[71] I. G. Kaplan, *Intermolecular Interactions: Physical Picture, Computational Methods and Model Potentials* (John Wiley & Sons, New York, 2006).

[72] M. Lepers and O. Dulieu, Long-range interactions between ultracold atoms and molecules, arXiv:1703.02833.

View publication stats